B.A.R.C.-1270

B.A.R.C.-1270

भारत सरकार

GOVERNMENT OF INDIA

परमाणु ऊर्जा आयोग

ATOMIC ENERGY COMMISSION

PROGRESS REPORT FOR (1974 - 1984)
NUCLEAR RESEARCH LABORATORY
SRINAGAR, KASHMIR

Edited by

P. K. Kaul and H. Razdan

भाभा परमाणु अनुसंधान केन्द्र

BHABHA ATOMIC RESEARCH CENTRE

बंबई, भारत

BOMBAY, INDIA

1985

B.A.R.C. - 1270

GOVERNMENT OF INDIA
ATOMIC ENERGY COMMISSION

B.A.R.C. - 1270

PROGRESS REPORT (1974 - 1984)

OF

NUCLEAR RESEARCH LABORATORY
BHABHA ATOMIC RESEARCH CENTRE
SRINAGAR, KASHMIR

edited by
R.K. Kaul and H. Razdan

BHABHA ATOMIC RESEARCH CENTRE
BOMBAY, INDIA
1985

INIS Subject Category : A 1560; B 3330; B 1400

Descriptors

COSMIC GAMMA SOURCES

GAMMA ASTRONOMY

COSMIC RADIATION

FORBUSH DECREASE

SOLAR ACTIVITY

GEOMAGNETIC FIELD

LIGHTNING

NEUTRONS

PARTICLE PRODUCTION

MOESSBAUER EFFECT

POLYMERS

ELECTRONIC EQUIPMENT

FABRICATION

ELECTRONIC CIRCUITS

GAMMA RADIATION

COBALT 60

CHEMICAL RADIATION EFFECTS

WOOD-PLASTIC COMPOSITES

RESEARCH PROGRAMS

BARC

CONTENTS

INTRODUCTION

Nuclear Research Laboratory was established at Srinagar in 1974 with a view to provide a base for planning and executing various research activities at the High Altitude Research Laboratory, Gulmarg, and to initiate applied research programmes in the field of Nuclear and Radiation Physics. The laboratory was initially set up in three barracks of the Regional Engineering College, Naseem Bagh, Srinagar and in 1976, was shifted to a private building, Samad Villa, Baghat Barzulla, Srinagar. In June 1981, the laboratory was finally moved to its permanent campus at Zakura, Srinagar. The first phase of laboratory construction is now over and a total space of 20,000 sq. ft. has been provided. The second phase of construction is being implemented and 38 staff quarters are being constructed on the campus.

Over the past ten years, research facilities in the following fields have been established at NRL.

1. Space Physics
2. Nuclear Physics
3. Radiation Chemistry and Atmospheric Chemistry
4. Technical Physics

At present the laboratory has a total staff strength of 80, which includes 25 scientists and 11 scientific assistants.

The report gives the highlights of the varibus research programmes undertaken at NRL, during the period 1974-1984. A list of papers published in various journals and presented at different conferences/symposia is given at the end.

1 Gamma Ray Astronomy

Cosmic gamma-rays, with individual photon energy $\geq$ 1 MeV, provide a unique diagnostic tool for the detection of cosmic ray sources in the galaxy and beyond. Gamma ray telescopes abroad SASII and Cos B satellites have already detected a number of possible point gamma - ray sources in the photon energy range $\leq$ 1 GeV. Further, more than 150 gamma-ray bursts have been detected in Vela and other satellites, with durations ranging from a fraction of a second to tens of seconds and sizes in the range 10^{-7} erg cm^{-2} to 10^{-3} erg cm^{-2}. It has not been possible to associate these bursts with any known astrophysical sources. On the other hand, gamma-ray bursts of micro-second duration have been predicted to accompany supernovae explosions and primordial black hole outbursts, but as yet there have been no positive observations of such bursts.

Recently, ground-based systems, employing the atmospheric Cerenkov technique (ACT) and the atmospheric fluorescence technique (AFT), have been used extensively for exploratory studies of gamma-ray bursts of duration $\leq$ 1ms and for the detection of discrete gamma-ray sources at $\geq 10^{12}$ eV. In both of these techniques, the atmosphere itself is used both as the target and the radiator and converts the incident gamma-ray photon into a shower of electrons, positrons, photons and nucleons. In ACT, electrons above

a certain threshold energy radiate Cerenkov photons in the visible and ultraviolet region, within $\sim 1^{\circ}$ of the direction of the radiating electron . The second method, AFT,makes use of the fluorescence properties of the atmosphere where electrons and photons of $\geq$ 1 keV energy produce excitation and ionization of nitrogen molecules, resulting in a pulse of visible radiation, the most prominent band being at 3914 Å from the first negative band system of N_2^+.

The main objective of the gamma-ray astronomy programme at NRL-HARL has been the exploration of the possible existence of short time-scale ($\leq$ 1 ms) cosmic x-and gamma-ray bursts through the atmospheric fluorescence technique and the detection of discrete point gamma-ray sources at high energies ($\geq 10^{12}$eV) through the atmospheric Cerenkov technique.

1.1. Atmospheric Fluorescence and Cerenkov Radiation Detection System at Gulmarg

C.L.Bhat, H.Razdan, M.L.Sapru, I.K.Kaul

An impulsive burst of gamma-rays (1MeV-1GeV) predicted to accompany a supernovae explosion or mini black hole evaporation, produces an atmospheric fluorescence radiation pulse, with a rise-time of $\sim$ 100 μs and a width of $\sim$ 1 ms, which is sufficiently intense to be detected against fluctuations in the night-sky background. Figure 1 gives the block diagram of the Gulmarg system employed to detect such a fluorescence pulse. It essentially consists of three

photomultiplier tubes, exposed to the night sky on clear moonless nights. Two of the photomultipliers are covered by violet filters (50% transmission in the 3400-4200Å band), while the third is covered with a yellow filter (50% transmission for $\lambda \geq 4300$Å). The differences in the temporal and spectral characteristics of atmospheric Cerenkov and atmospheric fluorescence radiation are utilized to identify the recorded pulses from the two processes and the data are then used to study the cosmic association of the recorded events.

A lightning channel is also incorporated in the system to monitor short time-scale ($\leq$ 1ms) variations in the atmospheric potential gradient and thereby help discriminate against optical events of lightning origin. The observed event profile, alongwith its absolute occurrence time provided by a digital clock, is recorded by a CRO-camera arrangement. The clock is maintained accurate to $\sim$ 1ms by regular time-synchronization with high frequency time-signals from ATA, New Delhi and RWM, Moscow.

Figure 2 shows an oscillogram of a typical atmospheric fluorescence pulse recorded by the Gulmarg system. It is characterised by negligible outputs in the yellow and lightning channels and a spectral ratio $Av/Ay \sim 5 \pm 1$, where Av and Ay respectively represent output pulse amplitudes in the violet and yellow filter channels. Out of a total of 109 candidate fluorescent events, recorded in 1674 hours of observation time, 96 are likely to be optical lightnings, whereas the other 13 represent candidate event for cosmic gamma-ray bursts. For two of these events recorded on Aug. 17, 1972 and Sept. 11, 1977, the occurrence

times are compatible with the event origin in optical supernovae detected in the galaxy NGC 735 and a faint spiral galaxy with right ascension 2h 01m and declination 11^{o} 43'. If these associations are correct, the temporal features of these events can be interpreted to imply that the supernova prompt photon burst has an overall duration $\geq$ 1ms and consists mainly of keV - GeV photons. On the other hand, if none of the recorded fluorescent events has a supernova origin, an updated upper limit (at 99% confidence level) of $\sim 5 \times 10^{46}$ ergs can be set on the prompt emission of gamma-rays from a supernova explosion.

1.2 Detection of Optical Bursts from Primordial Black Hole (pbh) Explosions:

C.L.Bhat, H.Razdan, M.L.Sapru

The terminal stage of the evaporation of a pbh is expected to be explosive and accompanied by the release of a burst of particles and gamma-rays. The collective interaction of these particles with the interestellar magnetic fields produces a coherent optical pulse ($E \simeq 10^{30}$ ergs, $\tau \sim 10^{-15}$ seconds, $M_{pbh} \simeq 10^{15}$ grams), which can be recorded by ground-based systems operating in coincidence over a long base-line.

An experiment to detect fractional microsecond duration optical pulses of possible cosmic origin, has been carried out by using two identical detector system at Gulmarg and Srinagar, separated by a distance of $\sim$ 30 Km. Each

system consisted of two 10" dia. photomultipliers, viewing the sky on clear moonless nights within a cone of 50° semivertical angle. In 74 hours of overlapping observations, while the number of observed coincidences for coincidence gate widths $\geq$ 5ms were compatible with random expectation, one optical pulse (rise time $\sim$200 ns, width $\leq$ 2 μs) was recorded simultaneously by the two systems (within $\sim$ 1 ms), as against a chance expectation of 0.14. Assuming this event to be a genuine pbh event, an upper limit of 0.33 events pc^{-3} yr^{-1} can be set on the pbh explosion rate. This value is an order of magnitude lower than the upper limit available at present.

1.3: A Non-Random Component in Cosmic Rays of energy $\geq 10^{14}$ eV.

(C.L.Bhat, M.L.Sapru, C.L.Kaul, P.R.Sarma)

The atmospheric fluorescence and Cerenkov radiation detection system, operated at Gulmarg during the period 1972-1977, has recorded Cerenkov light pulses from extensive air showers for nearly 70% of its on-time at the rate of $\sim$ 1 event/min. The extensive air showers are mostly initiated by cosmic ray protons of energy $\geq 10^{14}$ eV. Because of scattering by interstellar magnetic fields, the primary cosmic ray protons are isotropized in space and time and arrive randomly at earth, so that the arrival-time distribution of the events fits an exponential of the form $e^{-\lambda t}$ (λ= average event rate, t = time-seperation between successive events). Gamma ray initiated showers, on the other hand escape randomization because of the charge neutrality of the gamma-photon so that any periodic point

source of gamma-rays is expected to introduce a non-random contribution in the arrival-time distribution of the observed Cerenkov events.

The arrival-time distribution of $\sim$ 10,000 atmospheric Cerenkov events, recorded by the Gulmarg system, has been studied to investigate a possible non-random component. Figure 3 shows the observed distribution of time seperation t between consecutive events, on a 10 second bin size, alongwith the theoretical exponential fit to the distribution. The analysis reveals a 12% overabundance of events for $t \leq 40$ seconds. Figure 4 shows that the implied non-random component has a sidereal origin, because the high event rates exhibit a marked preference for the right ascension range 20 ± 03 hours. The results can best be explained in terms of the emission of ultrahigh energy gamma rays ($\geq 10^{14}$ eV) from one or more point sources in the general direction of the galactic plane.

1.4: A Very Long Baseline Search for Correlated Air Showers

C.L.Bhat, H.S.Rawat, H.Razdan, M.L.Sapru, S.C.Tonwar

Two air shower arrays were operated simultaneously at Gulmarg and Ooty (baseline $\sim$ 2500 Km), during Dec.1981 — Sept. 1982, to detect coincident air showers expected to be produced by cosmic gamma ray bursts of individual photon energy $\geq 10^{14}$ eV and relativistic dust grains emitted by pulsars. The use of a long baseline helps in reducing the chance

coincidence rate due to unrelated cosmic ray showers and eliminates local sources of noise, like lightning discharges etc. During 684 hours of overlapping observations, only one coincident event was observed within the ultimate time resolution of 1 ms, compared to a chance expectation of 0.7, thus making a genuine cosmic origin of the event unlikely. The number of coincident events observed for different coincident gate widths , in the range of 1 ms-1s, were also found to be comparable with the corresponding chance expectation due to background cosmic ray initiated showers. The results have been used to derive an upper limit of $\sim 10^{49}$ ergs on the prompt emission (within 0.1μs) of high energy gamma-rays (10^{9} eV-10^{14} eV) from supernovae explosions. Similarly, assuming that the terminal stage of primordial black hole explosion leads to the generation of a burst of $\geq 10^{14}$ eV gamma-rays, the upper limit on the pbh evaporation rate at 99% confidence level is estimated to be $\sim 3\times10^{-6}$ events pc^{-3} yr^{-1}. The present null result also leads to an upper limit of 0.1 events day^{-1} on the frequency of correlated air showers arising from the photo-disintegration of a relativistic dust grain emitted from a pulsar in the solar neighbourhood . Demanding that 4 extensive air showers be detected at each location within one minute to signify an event, the dust grain should comprise $\geq 10^{15}$ Fe atoms if it completely disintegrates into individual nuclei at a distance of 100 A.U. and gives a beam of particles of angular size 10^{-3} radians. This corresponds to a dust grain diameter of 1.5×10^{-3} cm. Further, taking the average galactic density of pulsars as 3×10^{-7} pc^{-3} and a power

law energy spectrum with a differential exponent of -2, we obtain a mass loss rate of 10^{-10} $M_\odot$ yr^{-1} from a pulsar in the form of relativistic dust grains of energy $\geq 10^{9}$ eV per nucleon. This leads to an energy loss rate of $\leq 10^{37}$ ergs s^{-1} in comparison with the total energy loss rate of 3×10^{38} ergs s^{-1} deduced for the Crab pulsar from its spin down rate, implying that the emission of relativistic dust grains may not be a dominant source of energy loss in the case of pulsars.

1.5: Possible Origin of Cosmic Gamma-ray Bursts in Globular Clusters:

H.Razdan, C.L.Bhat

A number of x-ray bursters, with burst energies and time scales similar to that of cosmic gamma-ray bursts (GRB) ; have been identified with galactic globular clusters. This fact together with the observation of an apparent lack of GRB sources in the galactic disk, suggests a possible origin of the GRB in globular clusters. To explore this possibility, a comparison of the size spectrum of GRB has been made with the spectrum expected if the bursts are generated within globular clusters, which form a spherical system of radius 20 kpc around the galactic centre. A spectral index of ~ 1.52 for the cluster size spectrum, for sizes $\geq 3 \times 10^{-6}$ ergs cm^{-2} , is in good agreement with the Vela and Imp 7 gamma ray burst data (Figure 5). Further significant positional association is also observed between individual gamma ray burst locations and the positions of globular clusters, especially in the case of GRB from high galactic latidues, showing thereby that the available observational data on GRB is compatible with their source location in globular clusters . It is suggested

that the preferential gamma ray burst activity in globular clusters at high galactic latitudes may result from the fact that the nuclear burning member of the binary system is in a comparatively late stage of evolution.

1.8: Pulsed Flux of 5×10^{14} eV Gamma Rays from Cyg.X-3

(C.L.Bhat, M.L.Sapru, H.Razdan)

A phase - histogram analysis of atmospheric Cerenkov pulses recorded during 1976-1977, by a wide-angle photomultiplier system at Gulmarg (India), has revealed a pulsed component of point-source origin, exhibiting the characteristic Cygnus X-3 modulation of 4.8 hours. Its amplitude is $2.6\pm0.3\%$ and duty cycle $\lesssim 5\%$, corresponding to a detected average flux of $(2.6\pm0.4)\times10^{-12}$ photon cm^{-2} s^{-1} at $\geqslant 5\times10^{14}$eV. Taken together with other spectral measurements (10^{4} - 10^{16} eV) from Cyg X-3, it suggests a long-term flux reduction by a factor of ≤ 2 per year for an assumed source distance of 11.6 kpc. The study also indicates that the fluxes detected earlier in the 10^{11} - 10^{12} eV region are anamolously lower, possibly on account of significant attenuation of the emitted gamma-rays through pair production interactions with the optical photon field around the companion star of the Cygnus X-3 binary system.

1.6: The Gulmarg Atmospheric Cerenkov Telescope

H.Razdan, C.L.Bhat, R.K.Kaul, R.Kaul, H.S.Rawat, M.L.Sapru, V.K.Sanecha, R.C.Rannot, A.K.Tickoo, R.A.Qazi, I.K.Kaul

An atmospheric Cerenkov telescope has been commissioned at Gulmarg to study cosmic gamma-ray sources at energies $\geq 10^{12}$ eV. The telescope at present employs six parabolic mirrors (90 cm diameter), coupled to 5" dia. fast photomultipliers and is divided into two independent telescopes of 3 mirrors each. The mirrors are fixed on equatorial mountings and are exposed to the sky on clear moonless nights to detect Cerenkov light pulses of $\leq$ 100ns duration. The telescopes are operated in the tracking mode and each mirror is capable of independent motion in both right ascension and declination. The system threshold has been estimated to be $5 \times 10^{-9} - 10^{-8}$ ergs cm^{-2} and extensive air showers. initiated by cosmic rays of energy $\geq 10^{12}$ ev have been registered at the rate of ~ 1 s^{-1}. The telescope has been used for a study of the possible gamma ray source 2CG195+04 (Geminga) and about 10 hrs. of data has already been collected.

1.7: Primary Cosmic Ray Energy Spectrum around 10^{15} eV

C.L.Bhat, H.Razdan, M.L.Sapru, P.R.Sarma

The two wide-angle photomultiplier (EMI9545B) system , exposed at Gulmarg on clear moonless nights, detects coincident Cerenkov light pulses from extensive air showers, initiated largely by primary cosmic ray protons.

The system threshold for shower detection has been determined from the fluctuations in night sky background and is $\sim 6 \times 10^{14}$ eV. A pulse height analysis of ~ 3000 events, observed during 60 hrs. of observations, indicates a break in the primary cosmic ray energy spectrum around 10^{15} eV, which persists even when the system field of view is restricted by collimators to exclude obliquely incident showers. Figures 6 and 7 show the integral pulse height spectra obtained with the two detectors, with separate least square lines fitted to the data points in each case. The fitted lines have slopes of 1.90 ± 0.02 and 2.20 ± 0.02 for detector 1 and 1.85 ± 0.02 and 2.20 ± 0.02 for detector 2, with the change-over in the spectrum occurring at 0.95×10^{15} eV and 1.04×10^{15} eV respectively. The results confirm the existence of a bend in the primary cosmic ray energy spectrum around 10^{15} eV and also demonstrate the capability of the atmospheric Cerenkov technique for the study of cosmic ray energy spectrum.

2. Cosmic Ray Modulation Studies

Observations of magnetic fields, solar plasma and cosmic rays in interplanetary space by satellite - borne detectors, alongwith the study of cosmic ray time variations on earth, have shown that cosmic rays can be used as a sensitive diagnostic tool for studying various solar phenomena and for probing the electromagnetic state of the inter-planetary space. Among all the ground-based cosmic ray detectors, neutron monitors are found to be the most suitable for the study of solar modulation of cosmic ray

intensity due mainly to their lower rigidity response. A large number of neutron monitors have been operating at various places all over the world and form a well distributed grid of stations. An IGY type neutron monitor, comprising 20 boron trifluoride counters with a total counting rate of $\sim$ 2,60,000 counts hr^{-1}, has been operating at Gulmarg since 1969. The main objective of the cosmic ray modulation studies at NRL is the study of cosmic ray diurnal anisotropy characteristics during both electromagnetically quiet and disturbed periods and the investigation of the origin of Forbush decreases, by studying the plasma and magnetic field configuration of interplanetary space following the occurrence of solar flares and recurrent high speed solar wind streams. The relationship between active regions and solar coronal holes has also been studied by the analysis of ground-based cosmic ray data.

2.1 Anomalous Cosmic Ray Diurnal Anisotropy:

H.Razdan, M.M.Bemalkhedkar

The Gulmarg neutron monitor data and data from the worldwide network of neutron monitors has been used to study the characteristics of cosmic ray diurnal anisotropy on a daily basis. The study has revealed the existence of a new type of enhanced diurnal anisotropy, designated as Anamolous Diurnal Anisotropy, which occurs during the recovery phase of Forbush decreases. As shown in Figure 8 the anamolous diurnal anisotropy exhibits large amplitude of $\sim$1% (as against an average value of 0.4%)and has a time of maximum in the 0900 hour direction in interplanetary space, as compared to a maximum in the 1800 hour direction in the case of the average co-rotational anisotropy. The Forbush decreases preceding the days of anamolous diurnal anisotropy are found to be associated with 27-day recurrent solar M.-region streams and are in some cases preceded by east limb solar flares. The results have been explained in terms of an enhanced ontward convection of

cosmic ray particles and inward diffusion along the garden hose direction in the presence of a transient modulating region from a corotating stream. The various cosmic ray streaming vectors which lead to anamolous diurnal anisotropy are illustrated in Figure 9 .

A study of cosmic ray diurnal anisotropy on a day-to-day basis has revealed that on $\sim$ 4% of the days, the diurnal anisotropy exhibits anamolous behaviour, with the time of maximum in the 6-12 hour direction in inte. planetary space. This quiet-time anamolous diurnal anisotropy generally exhibits low amplitudes ($\sim$ 0.2%)and is found to occur in groups of several days which are not associated with enhanced solar wind velocity or solar cosmic ray emission. A model of the electromagnetic state in the interplanetary space has been built to explain the quiet-time anamolous diurnal anisotropy in terms of a significant contribution to the streaming from field perpendicular diffusion in the solar equatorial plane and the simultaneous additional streaming due to helio-latitudinal cosmic ray density gradients.

2.2: Long Term Modulation of Cosmic Ray Diurnal Anisotropy

R.K.Kaul, H.Razdan, M.M.Bemalkhedkar, C.L.Bhat

Cosmic ray diurnal anisotropy has exhibited a very anamolous behaviour during the solar minimum period of 1954, when for a period of three months (July-September, 1954), the time of maximum shifted towards early morning hours and the amplitude reduced to a negligibly small value. This effect was not observed 11 years later, during the solar minimum activity period in 1965. Using the data from Gulmarg neutron monitor, together with the data from the worldwide network of monitors, a study was conducted to investigate the possible 22-year recurrence tendency of the anamolous diurnal anisotropy. It was observed that the diurnal anisotropy observed by high threshold rigidity monitors (Gulmarg and Tokyo) exhibited a morning maximum on a large number

of days during July-September 1976, leading to negligibly small amplitudes of the mean monthly vectors, similar to that observed in the case of low threshold rigidity monitors during Feb.-March 1977, suggesting that the anamolous diurnal anisotropy observed at solar minimum epochs is 22-year recurrent. The observed anamolous diurnal anisotropy has been related to the occurrence of a preferentially unidirectional interplanetary magnetic field configuration (absence of sector structure) around the solar minimum periods and the resulting $B \times \nabla N$ streaming due to heliolatitudinal density gradients.

2.3: Study of the August 1972 Forbush Decrease Events:
(S.P.Agarwal, A.G.Ananth, M.M.Bemalkhedkar, L.V.Kargathra, U.R.Rao, H.Razdan)

A series of spectacular cosmic ray events, which include two relativistic solar particle enhancements and three major Forbush decreases, was registered during Aug. 4-9, 1972. Figure 10 shows the cosmic ray intensity variation recorded by the neutron monitors at Gulmarg and Ahmedabad and the meson monitors at Ahmedabad, during this period. The three Forbush decreases exhibited interesting and complex behaviour, including the occurrence of a pre-increase and a universal time increase. A model has been developed to explain these features in terms of a transient modulating region associated with the passage of a shock front. Evidence from interplanetary plasma, radio and magnetic field measurements supports the proposed model, Figure 11 summarizes the essential features of the model which involves a region of high tangled magnetic fields behind the leading edge of the shock front, where the cosmic ray particle flux is highly depressed. Immediately behind this region is a region of enhanced particle flux, with sharp density gradients, followed by the main magnetic cavity with well-ordered magnetic fields and depressed particle density. The cosmic ray intensity within the cavity recovers exponentially with time and ground-based monitors observe different cosmic ray intensity

variations as the cavity convects past the earth.

2.4: Origin of Cosmic Ray Forbush Decreases and their Association with Solar Flares, High Velocity Solar Streams and Interplanetary Magnetic Blobs

(G.N.Shah, C.L.Kaul, H.Razdan)

Transient decreases in cosmic ray intensity known as Forbush decreases, are believed to result from solar plasma and magnetic field disturbances propagating through interplanetary space. A statistical study of Forbush decreases, observed by ground-based monitors during the period 1966-1975, has revealed , that in addition to solar flare plasma, high velocity solar wind streams also lead to such decreases. Classifying Forbush decreases into recurrent and non-recurrent categories, on the basis of their recurrence with respect to interplanetary magnetic field blobs of duration $\geqslant$ 4 hours, it has been shown that unlike in the case of a recurrent decrease, a non-recurrent decrease is always preceded (within 10-100 hours) by a flare of importance $\geqslant$ 1B /2N. The results can best be understood by assuming that non-recurrent decreases are primarily caused by flare-initiated disturbances whereas recurrent decreases are caused by high velocity solar wind streams. In case a flare is observed to precede a recurrent decrease, the cosmic ray intensity time profile is modified due to the simulteneous presence in interplanetary space of a modulating plasma cloud both from the flare and the corotating stream (Figure 12).

Analysis of Forbush decreases has also been carried out in relation with the interplanetary magnetic field and plasma data, obtained from various earth-orbiting satellites during the period 1966-1975. Figure 13 shows the superposed epoch analysis of the hourly values of solar wind velocity, plasma density and magnetic field strength in the interplanetary space, with the onset time of Forbush decrease as the epoch. The significant differences between the three sets of data, corresponding to non-recurrent decreases initiated by flares, recurrent decreases not preceded by flares and recurrent

decreases preceded by flares respectively, can be explained on the basis of flare and/ or stream plasma sweeping past the orbit of earth at the Forbush decrease onset time.

2.5: Forbush Decreases, Interplanetary Magnetic Field Blobs and Coronal Holes

G.N.Shah, C.L.Kaul, H.Razdan

A study of the relationship between cosmic ray Forbush decreases and the interplanetary magnetic field has revealed that the onset of a Forbush decrease is always preceded by the passage of an interplanetary magnetic field blob across the earth's orbit. However, this alone does not seem to be a sufficient condition for the occurrence of a Forbush decrease, because a large number of well-defined magnetic blobs did not produce any decrease in cosmic ray intensity during 1966-1975. Further, the Forbush decrease amplitude is neither correlated with the peak intensity in the magnetic blob nor with the magnetic field gradient at the leading edge of the blob (Figures 14 and 15).

Forbush decreases have also been studied in relation to solar coronal holes for the period 1972-1974. It has been shown that while the majority of coronal hole passages are followed by geomagnetic storms, only a few coronal hole passages are followed by Forbush decreases. The Forbush decrease initiating coronal holes are observed to be asociated with solar wind streams having large velocity gradients, high ion density and high magnetic fields at their leading edges. Some common interplanetary features present during the stream - associated and flare-associated decreases, like interplanetary magnetic field structure, dominant peak in ion density and solar wind velocity gradients etc., have been identified. In particular, the B_z component of interplanetary magnetic field is found to attain large negative values in the case of coronal holes followed by Forbush decreases.

2.6: Distribution of Active Regions on the Sun:

(G.N.Shah, C.L.Kaul, H.Razdan)

Active regions are the sources of solar flares

which produce important effects in terrestrial atmosphere,geomagnetic field and interplanetary space. For a detailed understanding of their birth and decay, an attempt has been made to study the active region distribution on sun, for $\sim$ 120 solar rotations, covering the period 1965-1974. It has been shown that for extended periods of time, during solar cycle 20, the solar active regions were mainly confined to two longitude zones $\sim 180^{o}$ apart (Figure 16). The clustering of active regions appears to be more pronounced in the northern than in the southern hemisphere of the sun, which in the light of earlier results obtained for solar cycle 19, suggests the existence of a hemispherical asymmetry in the distribution of active regions that reverses with a period of $\sim$ 11 years. Further, the two longitude zones of active regions are found to shift by $\sim 6^{o}$ per solar rotation to the east of their previous locations (Figure 17).

2.7: Relation Between M-regions and Active Regions:

(G.N.Shah, C.L.Kaul, H.Razdan, M.M.Bemalkhedkar)

M-regions are the quasi-permanent regions on sun, devoid of any physical features, which are responsible for 27-day recurrent geomagnetic disturbances. Satellite observations have shown that M-region initiated geomagnetic storms are usually accompanied by recurrent Forbush decreases and high velocity solar wind streams. Utilizing worldwide observations on cosmic rays, it has been shown that the onset of a 27-day recurrent M-region disturbance in cosmic rays is accompanied by the presence of a class of active regions near the central meridian of sun, which frequently give rise to solar flares of importance $\geq$ 2B/3N (Figure 18). Making use of the quasi-radial hypervelocity approximation for solar wind propagation, the base of the leading edge of the high velocity solar wind stream from the M-region has been traced to $\sim 40^{o}$ W of the central meridian of sun. From these results it is condluded that M-regions lie preferentially to the west

of large active region complexes. Since active region complexes have been shown to shift to the east of their previous locations by $\sim 6^{\circ}$ per solar rotation, it suggests that M-regions are born to the west of active regions, at the sites where old active regions are decaying to form open magnetic field structures. Such field configurations are favourable for the formation of high velocity solar wind streams, a characteristic feature of M-regions.

3. SOLAR TERRESTRIAL RELATIONSHIPS:

Solar flares, sun spots, high velocity solar wind streams and the interplanetary magnetic field sector structure are various manifestations of disturbances occuring on the sun, which have a profound effect on the earth's magnetic field and upper atmosphere. A number of convincing findings have also appeared that link the earth's weather to solar and interplanetary parameters. The research activities of NRL have mainly focussed on the study of the various aspects of solar activity and the interaction between solar radiations and terrestrial atmosphere. Some interesting results have been obtained in the field of sun-weather correlations and the asymmetrical effect of solar disturbances on the northern and southern hemisphere geomagnetic field.

3.1: Solar Proton Events and Terrestrial Weather:

G.N.Shah

The study of the effects of energetic solar particle influx into the earth's atmosphere on Vorticity Area Index (VAI) has proved very useful in the recent sun-weather correlation studies. The response of atmospheric Vorticity area index to solar proton events for a period of 19 years (1954-1972), has revealed that VAI reaches a minimum one day after the entry of high energy solar protons into the earth's atmosphere. In contrast with the other sun-weather correlations reported so far, the decrease in VAI ($\sim$ 11%) is observed only during the summer months (Figure 19).

The effect is seen consistently during the period 1954-1969, covering full solar cycle 19 and the first half of solar cycle 20. The analysis further reveals that the period 1970-1972 does not show the behaviour seen for the rest of the period (1954-1969), suggesting that the sun-weather effect may have undergone a change during 1970-1972.

3.2: Asymmetry in the Response of Geomagnetic Field to Solar Disturbances:

(G.N.Shah, R.K.Kaul,C.L.Kaul, H.Razdan, W.M.Wilcox, W.Merryfield)

Geomagnetic activity has been suggested as a possible link in sun-weather correlations. Since some sun-weather relationships, especially the VAI - Sector boundary crossing effect , seem to exhibit seasonal and hemispherical asymmetries, an attempt was made to study the possible existence of similar asymmetries in geomagnetic activity. For this purpose, the onset times of solar proton events, solar flares and cosmic ray Forbush decreases were chosen as the indicators of solar activity and the behaviour of magnetic activity indices ap, an and as following solar disturbances was studied. The results indicate that the geomagnetic field is more prone to disturbances around the June solstice than around the December solstice, as evidenced by a larger enhancement in geomagnetic activity following the onset of transient solar disturbances occurring in the 3-monthly period around 21 June than in the corresponding period around 21 December (Figure 20). Further, an asymmetry between the northern and southern hemisphere geomagnetic activity is also exhibited independent of the level of activity. As shown in Figure 21 , the hemispherical asymmetry exhibits a regular annual variation with a maximum of 60% around June solstice and is almost absent around December solistice showing the inherently larger susceptibility of northern hemisphere geomagnetic field to solar disturbances. The reason for such an effect needs to be explored further.

3.3 : Effect of Cosmic X-ray Source Tau X-1 on D-Region Ionization

(R.K.Kaul, H.Razdan)

A long wave (LF) propagation experiment was conducted at Gulmarg during the period 1974-1980, to examine the possibility of detecting cosmic x-ray sources through their ionospheric effects. The technique involves the measurement of the signal strength of 1-hop signals from the 164 KHz CW radio transmissions from Radio Tashkent and correlating the observed signal strength variations with the transit of various cosmic x-ray sources. Increased absorption of the 164 KHz waves, corresponding to increased D-region ionization at the time of the transit of Tau x-1 over the Tashkent - Gulmarg reflection point, was observed consistently during the period 1975-1977, as depicted in Figure 22 . On a day to day basis, the signal minimum observed at the time of Tau X-1 transit, is shown to exhibit a sidereal time shift of $\sim$ 4 minutes/day (Figure 23), indicating that the signal minima are indeed associated with the transit of Tau x-1. The observed absorption has been shown to depend on the level of ambient ionization, possibly due to a variation in the mesospheric nitric oxide concentration with geomagnetic activity.

3.4: Charged Particle Measurements in Space from OGO-VI Albedo Neutron Detector

(R.K.Kaul, H.Razdan, J.A.Lockwood)

The University of New Hamisphire, U.S.A., neutron detector on board OGO-VI satellite had an anticoincidence shield of charged particle detectors, which formed an omnidirectional charged particle detector of large geometrical factor (950 cm^2 str)and energy thresholds of $\geqslant$ 1.5 MeV for electron and $\geqslant$ 13 MeV for proton detection. Analysis of the charged particle data on various satellite orbits has revealed the existence of a quasi-permanent ring of MeV energy particles around the earth's equator, with fluxes of $\sim$ 50-70 particles m^{-2} s^{-1} str^{-1}. This ring of quasi-trapped particles was found to lie below the inner radiation belt

parison of the observed fluxes with earlier measurements revealed a power law energy spectrum for these particles (Figure 24)with an exponent of ~ -3. These particles have been attributed to outer belt protons lost through charge exchange process, the neutral hydrogen being reconverted into protons at low altitudes through charge exchange with atomic oxygen.

The charged particle data from OGO-VI was also used to estimate the cosmic ray radial density gradient. For this purpose, charged particle fluxes measured in the polar regions ($\lambda_m \geq 80^{\circ}$) were corrected for the altitude variation and the contribution from splash and re-entrant albedo, to yield a flux of 2.858+0.008 particles cm^{-2} s^{-1} at 1000 Km altitude. A comparison of this value with the Pioneer VI measurements of the cosmic ray flux in deep space, leads to a value of 6.92 ± 2.0 %/A.U for the cosmic ray radial density gradient.

3.5: Non-Magnetospheric Origin of Fast Atmospheric Pulsations

(C.L.Bhat, M.L.Sapru, R.K.Kaul)

Analysis of $\sim$ 30,000 optical pulses of atmospheric origin, with time-scales $\leq$ 1ms, recorded in the Gulmarg atmospheric fluorescence detector, has revealed that the so-called fast atmospheric pulsation events recorded in similar experiments elsewhere, cannot be attributed to radiation belt particles precipitated into the atmosphere. It has been shown that the temporal and spectral characteristics of the fast atmospheric pulsation events are not compatible with that expected for atmospheric fluorescence radiation excited by photons and charged particles of $\geq$ 1 KeV energy. It has been suggested that the reported fast atmospheric pulsation activity may represent a form of local noise, produced at low altitudes in the atmosphere and most probably of man-made origin.

4. Neutron Generation in Lightning Discharges:

(G.N.Shah,H.Razdan, C.L.Bhat, Q.M.Ali, S.R.Kaul)

Intense electric discharges through thin, deuterium enriched polymer fibers have been shown to generate 2.45 MeV neutrons by Deuterium-Deuterium fusion. Based on the broad similarities between laboratory discharges and natural lightnings, the generation of such neutrons in lightning flashes at yields of $\sim 10^5$ neutrons/lightning stroke, has been predicted . An earlier experiment, using fission track detectors placed near lightning arrestors, has failed to confirm neutron production in lightning discharges. A modified IGY type neutron monitor was used at Gulmarg , during the period 1980-1984, for the possible detection of neutrons from individual lightning strokes for a time interval comparable with the actual duration of the discharge ($\sim 320\ \mu s$) during which the cosmic ray neutron background is almost zero.

The mean energy response of the neutron monitor at Gulmarg has been reduced to a few MeV by removing the lead completely and by reducing the thickness of the paraffin wax moderator. This modified low energy neutron monitor comprises 21 boron trifluoride counters, each 90 cm long and 3.8cm in diameter, spread in the form of a pile, on 28 cm thick paraffin wax slabs of surface area $3 \times 10^4\ cm^2$, and covered on top with 8.5 cm of paraffin, sufficient to thermalize neutrons of 2.5 MeV energy. The monitor has an integrated count rate of $\sim$ 36000 counts per hour (statistical error = 0.53%) and continuously monitors the low energy atmospheric neutron background. Figure 25 shows the variation of observed count rate as a function of atmospheric pressure, the pressure coefficient being $\sim$ -0.7%/mb.

Figure 26 shows the experimental arrangement used for the detection of neutrons from lightning discharges. The lightning stroke is sensed by recording the electromagnetic pulse, which activates a clock to record the time

till the first neutron is detected in the pile. This in turn activates a sequential counter in which any neutrons subsequently reaching the detector are counted in four identical gates of total width 320 μs. The time delay between the detection of the electromagnetic pulse and the detection of the first neutron in the pile, alongwith the number of neutrons detected during 320 μs is recorded on a printer. The former gives an estimate of the distance to the lightning stroke and the latter enables the evaluation of the neutron yield from the lightning stroke. Since the cosmic ray background neutron rate in 320 μs is negligibly small, such a mode of operation gives a high signal to noise ratio.

During the period May 1980- May 1983, the system was triggered 11,200 times by lightning discharges. During the same period it was also triggered manually on 8,400 occasions by feeding a pulse to the electromagnetic channel at randomly chosen epochs. The time distribution of single neutron events is shown in Figure 27 . Exponential curves fit both the data sets (Lightning triggered events and manually triggered events) and yield a count rate of $\sim$ 10/s, which is the background count rate of the monitor. This indicates that single neutron events are not related to lightning discharges and are only cosmic ray background neutrons.

Table 1 compares the frequency of lightning triggered (LT) events as a function of neutron number recorded per event, with the corresponding number of manually triggered (MT) events. There are only 4 MT events recorded with 3 neutrons/event and none with $\geqslant$ 3 neutrons/event. On the other hand, 124 LT events have been registered with $\geqslant$ 3 neutrons/event including 59 events with $\geqslant$ 6 neutrons/event and 39 events with $\geqslant$ 9 neutrons/event respectively. The large differences in the relative number of LT and MT events and in the neutron yield/event, show that the LT events

with $\geqslant$ 3 neutrons/event must be associated with the lightning discharges. The distance to the causative lightning discharge has been calculated from the measured time-delay between the detection of the electromagnetic pulse and the first detected neutron and is used to derive a neutron yield of $8.8 \times 10^{6} - 2 \times 10^{10}$ neutrons/stroke for 64 events, assuming the neutron energy to be 2.5MeV. The results provide the first positive evidence for neutron production in natural lightning discharges.

5. Nuclear and Solid State Physics:

A programme to study a variety of organometallic polymers, through Mossbauer spectroscopy, was initiated at NRL in 1974. Metallopolymers can play an important role in various biological systems and because of their characteristic semiconductor and dielectric properties, may also have potential applications in the field of electronics.

A constant velocity Mossbauer spectrometer with a loud speaker drive system was installed at NRL in 1974. A series of new metallopolymers were made at NRL from various monomers, with the aim of studying long range effects and $\sigma-\pi$ interactions. To start with, polymetallomethacrylates and acrylates were made with Fe^{57} as the probe and other metals (Zn, Ag, Pb etc.) were introduced in the monomer and were subsequently polymerised by gamma-irradiation.

5.1: A Constant Velocity Mossbauer Spectrometer Free of Long Term Instrumental and Radioactive Decay Drift

(P.R.Sarma, K.C.Tripathi, A.K.Sharma)

In the Mossbauer spectroscopy of polymer samples, which generally contain a small percentage of the Mossbauer absorber, measurements over a long time become necessary to get a spectrum of good statistical quality. It is, therefore, imperative that long term instrumental drifts and radioactive decay drifts be avoided in a constant velocity loud speaker type drive system. Two new control circuits were developed to avoid both these types of drifts. The circuits generate a staircase type waveform instead of the square wave form in the conventional drive system, so that in each oscillation the source remains stationary for a fraction of the time period. The gamma rays counted during this period are monitored alongwith positive and negative velocity counts and are used to correct any fluctuations in the count rate by feeding these pulses in the timer. Figure 28 shows a comparison

of Mossbauer spectrum of sodium nitroprusside taken with the conventional (loud speaker drive system) and the modified drift free system.

5.2: Mossbauer Studies on Polymetallomethacrylates:

(K.C.Tripathi, P.R.Sarma, H.M.Gupta)

Poly-iron-methacrylate and poly-iron-zinc-methacrylate were studied by Mossbauer spectroscopy at room temperature. The samples were prepared by reacting methylmethacrylic acid as monomer with Ferric chloride and irradiating the product with Co^{60} gamma-rays. Mossbauer spectra were taken using 1.5 mc ^{57}Co source, absorber thickness of about 2.5 mm and effective counting time of $\sim$ 300 hours, using the constant velocity drive system. Comparison of the two spectra (Figure 29) indicates that the introduction of zinc in addition to iron in the polymer perturbs the system effectively. Since zinc and iron are well separated and the only link between them is through the polymer chain, the results indicate presence of a long range interaction. Thus even the distant groups exert a strong inductive effect on the electron shells and the functional group in which iron is located has a strong inductrometric polarizability.

5.3: Mossbauer study of the gamma-induced Polymerisation of Iron-methacrylate and Iron-acrylate

(P.R.Sarma, H.M.Gupta, K.C.Tripathi)

A Mossbauer spectroscopic study of the gamma-induced polymerisation of iron-methacrylate and iron-acrylate has been conducted. Iron-methacrylate, a solid monomer in powdered form, was produced by reacting iron-hydroxide with methacrylic acid and polymerised by irradiating with a ^{60}Co gamma-ray source, while iron-acrylate was produced by reacting iron hydroxide

with acrylic acid, followed by gamma-irradiation. A number of Mossbauer spectra were taken after subjecting the samples to different cumulative doses of gamma-rays. The iron-methacrylate spectra were found to be asymmetric doublets, with the percentage asymmetry, $(I_1 / I_1 - I_2)$, a function of the period of irradiation (Figure 30). The changes in asymmetry have been correlated with the degree of polymerisation determined independently by chemical analysis and resistivity measurements. In iron acrylate, the gamma-absorption is seen to change with the degree of polymerisation. The results indicate the occurrence of cross linking in iron acrylate and degradation in iron methacrylate by irradiation after maximum polymerisation.

5.4: Mossbauer Study of the Copolymers of iron and Nickel methacrylates in methacrylic acid:

(P.R.Sarma, K.C.Tripathi, H.M. Gupta)

The paramagnetic relaxation in the system poly (iron methacrylate)x (nickel methacrylate)2.5-x (methacrylic acid) 97.5 for x = 0.2, 1.5, 2.0 and 2.5, has been studied through Mossbauer spectroscopy at room temperature. Iron methacrylate and nickel methacrylate were produced by treating iron hydroxide and nickel hydroxide respectively with methacrylic acid. The copolymers were made by mixing the monomers in various proportions and then polymerising the mixture by γ -irradiation with a ^{60}Co source. Figure 31 shows the Mossbauer spectrum for x = 2. For pure iron methacrylate in the acid, the spectrum is an asymmetric doublet. In the presence of nickel methacrylate, relaxation spectra are obtained. As the concentration of iron decreases, the intensity of the line at zero velocity decreases and hyperfine lines begin to resolve. With the change in iron concentration, the spin-lattice relaxation time remains unchanged and

only the average distance between the ferric ions changes, so that the observed relaxation effects can be attributed to a spin-spin interaction.

5.5: Optimisation of Absorber Thickness for High Signal-to-noise Mossbauer Spectra

(P.R.Sarma, V.P.Gupta, K.C.Tripathi)

The optimum thickness of a single line Mossbauer absorber, which will yield in a given experimental time a Mossbauer spectrum having the highest value of signal-to-noise ratio, has been calculated. A simple formula for the optimum thickness has been derived for the particular case where the line widths of the source and absorber are almost equal and the lines are Lorentzian in shape. Figure 32 depicts the variation of optimum thickness T_o as a function of the effective mass absorption coefficient λ ($gmcm^{-2}$) for various values of the parameter β (function of the line widths of source and absorber).

5.6: Scattering Geometry Mossbauer Effect:

(P.R.Sarma, K.C.Tripathi, M.R.Singh)

An analytic expression for the thickness dependence of the line width of a scattering Mossbauer single line spectrum has been derived. Starting from the line shape calculated by Bara and taking into account all significant scattering phenomena (Rayleigh and Compton scattering, resonant and non-resonant absorption etc.), an expression in the form of a Taylor series expansion, in terms of the thickness of the scatterer has been obtained for thin scatterers.

6. Energy Dispersive X-ray Fluorescence System for Trace Element Analysis

(G.S.Lodha, R.Koul, K.J.S.Sawhney, H.Razdan)

An energy dispersive x-ray fluorescence (EDXRF) Spectrometer, consisting of Si(Li) detector and an ECIL make 4k multichannel analyser, has been set up at NAL. For a mass storage of data and on-line computation of stored spectrum, the system has been coupled to a Hindustan Computers Ltd. Micro 2200, having a floppy disk drive attachment. The block diagram of the system is shown in Figure 33.

The 30 mm^2 x 3 mm Si(Li) x-ray detector, mounted in a cryostat, is cooled to liquid nitrogen temperature and employs a drain feedback FET preamplifier, the first stage of which is also cooled to liquid nitrogen temperature. Energy resolution of 220 eV at 5.9 keV is achieved with this system. Low energy radioisotopes and a low power laboratory built x-ray tube are being used for the excitation of characteristic x-rays in the samples. Another Si(Li) x-ray detector system, having an energy resolution of 153 eV at 5.9 keV and employing pulsed optical feedback preamplifier has also been set up and has been coupled to Canberra 85 programmable multichannel analyser.

6.1: Study of Geochemical Profiles in Kashmir Loess Deposits:

(G.S.Lodha, K.J.S.Sawhney, R.Kaul, H.Razdan)

In recent years, interest has been shown in the trace element analysis of Loess and paleosol deposits, with a view to understand the gross features of the climate over the past several million years. The

climatic record of the Kashmir valley for the past four million years is preserved in Karewa sediments, having an estimated thickness of about 1000 meters, which have got exposed due to the uplift of Pirpanjal mountains by plate tectonics. The x-ray fluorescence system at NRL has been used to study the trace element concentration in loess and paleosol deposits in Kashmir valley and the distribution, migration and accumulation of various constituent trace elements. The study is expected to provide an insight into the geochemical environment of loess accumulation.

Concentration values of K, Ca, Ti, Mn, Cu, Zn, Rb, Sr, Y, Zr, Nb, Ba, La and Ce have been computed for loess and paleosol samples from Kanchinala section, Kashmir (Figure 34). The elements related to plant activity (Mn, Cu, Fe) are found to have generally higher concentration in paleosols compared to loess deposits. The distribution of these elements in paleosols is closely related to soil formation. The distribution of Rb, Ba and Zr indicates uniformity of composition of loess columns whereas the higher values of Mn, Cu, Fe and lower values of Sr in paleosols provide markers for identification and confirmation of paleosols. The sediments derived under extremely cold conditions are known to have higher concentrations of Sr. Thus the relative fractionation of Sr from loess to paleosol layer may provide a picture of intense climatic variations.

6.2: Concentration Profiles of Trace Elements in Dal Lake Sediments:

(G.S.Lodha, K.J.S.Sawhney, R.Kaul, H.Razdan)

Trace element concentration profiles of sediments can be a sensitive indicator of the effects of natural and man-made activities on Dal Lake ecology. A study of the trace element concentration

in surface sediments from the Hazratbal basin of Dal Lake was conducted to study the distribution profiles of Ca, Ti, Cr, Fe, Cu, Zn, Pb, As, Rb, Sr, Zr and Ba by the EDXRF system at NRL. The concentration values of Ca around the banks of Hazratbal Park were found to vary from 2.4% to 3.1%, which is almost an order of magnitude higher than the range of concentration values (0.1% to 0.3%) found in other parts of the basin (Figure 35). This may probably be due to the high ratio of run off from the banks, due to the higher population density in the area. The concentration values of Cu near the 'floating' gardens were found to be in the range 27-49 ppm, which are lower than the value of 51-73 ppm in other parts of the lake. A similar trend was observed in the case of Zn and Fe. The lower concentration of Cu, Fe and Zn around the 'floating' gardens implies that the sediment load from these areas is continuously used for building the 'floating' gardens, where these elements are being taken up by the plants and vegetables grown there.

The concentration of Zr was observed to be in the range 400 - 500 ppm near the Telbal and Shalimar nallahs, which are the main inlets to the lake. These values are higher than that found in the other parts of the lake and indicate that the sediment load from the Telbal and Shalimar nallahs is slightly richer in Zr.

6.3: Studies on the Wear and Tear of Machines:
(G.S.Lodha, R.Kaul)

A study was undertaken to look into the possibility of using the EDXRF system as a tool for

monitoring the wear and tear of machines with moving parts. Element concentration of the used cryogenerator oil of the Philips Liquid Nitrogen Plant (PLN - 106) was compared with the elemental concentration of fresh oil. A sample of fresh oil was observed to have only minute traces of iron which, however, increases as the machine is used for longer periods. A fixed rate of increase in the contamination of the lubricating oil for different machines was observed, so that an increase beyond the permissible level can be used as a signal indicating the imminent breakdown of the machinery.

7. Electronics and Technical Physics:

A number of electronic test instruments and other equipment have been designed and fabricated for use in the various experimental programs. Some of the main instruments developed are described below :

7.1: High Voltage Regulated Power Supply for X-ray Tubes:

(M.M.Bemalkhedkar, C.M.Tripathi, M.N.Kumbare, H.S.Vora)

A solid state power supply unit, incorporating three regulated and adjustable power supplies required for the operation of the X-ray tube in the energy dispersive x-ray fluorescence system (section 6), has been designed and fabricated. The three supplies include a 40 KV/0.5 mA H.T. supply, a 500 V/1mA grid bias supply and a 12V/8A filament supply (Figure 36). All the supplies have excellent temperature stability from 15°C to 50°C and the H.T. supply has a very low ripple of $\leq$ 0.05%. Figure 37 illustrates the characteristics of the H.T.supply. The H.T. and bias supply are basically dc-dc converters utilizing driven push-pull inverters

followed by a voltage multiplier, filter and bleeder configuration. The unit has been successfully integrated into the EDXRF system operating in the laboratory.

7.2: Low Voltage Regulated D.C.Supply with Digital/ Analog Control for Firing SCR's

(M.M.Bemalkhedkar, R.Koul, C.M.Tripathi, M.S.Qureshi, M.N.Kumbhare)

A low voltage regulated power supply with new design features has been built. It employs full wave rectification by silicon controlled rectifiers (SCR's), with the firing angle controlled by digital circuits to provide improved output voltage stabilization. Figure 38 shows the circuit diagram of the modified power supply and Figure 39 depicts its performance characteristics. Output voltage stabilization is achieved by comparing a fraction of the output voltage with a reference voltage and using the error signal to vary the frequency of a voltage controlled oscillator (VCO), which determines the period or the firing angle of the SCR's. A similar power supply using an analog feedback circuit has also been designed and fabricated.

7.3: Digital Display Photometer for Visible Photon Flux Measurements:

(H.S.Vora, T.N.Das, M.N.Kumbhare)

An integrated digital display and recording type photometer has been developed for the continuous monitoring and recording of the sky light photon flux. Figure 40 shows the circuit diagram of the system. Using silicon photo diodes as the photon sensors, the changes in the frequency of a free-running multivibrator are monitored for a preset

time to give the photon flux directly. The duration of each measurement is manually adjustable over four orders of magnitude in time. The system responds linearly to incident photon flux variations over at least seven orders of magnitude. Absolute calibration of the system has been done with a thermopile as well as with a fixed frequency laser. The photometer is being used in the study of atmospheric photochemical reactions.

7.4: Logic Pulse Generator

(C.L.Bhat, R.C.Yadav)

An inexpensive digital pulse generator with pulsewidth, period and delay adjustable from 0.1 μs to 10 s, in steps of 0.1 μs, has been designed and fabricated. The system design provides an LED display of the preset pulse parameters. Figure 41 gives a schematic diagram of the circuit operation. Gate 1 always remains open and the high frequency oscillator continuously feeds the frequency divider D. At the two tappings on D, two pulse trains PT1 and PT 2 (PT2 slower than PT 1) are generated. PT2 repeatedly opens gate 2 which is subsequently closed each time by the output of preset counter C. A pulse is, therefore, generated at the output of gate 2, with a width equal to the time for which the preset counter C counts and with a repetition rate equal to the output pulse train of divider D. If the output of the preset counter is once more gated through another gate with PT2 pulse trains with repetition frequency of PT2 can be generated. In the manual mode of operation, gate 1 is opened manually and closed by C to give one pulse or a pulse train each time. Figure 42 gives the actual circuit diagram of the pulse generator.

7.5: An Error Monitoring and Correction Circuit for Clocks:

(C.L.Bhat, H.Razdan, M.L.Sapru, I.K.Kaul)

A logic synchronization circuit has been developed , which monitors and corrects clock errors of $\leq$ 500 ms in mode A with the help of time-code signals from ATA, New Delhi and RWM, Moscow. In mode B, additional logic circuit incorporated in the system, extends the correction range to $\pm$ 30s. A schematic view of the logic operation is shown in Figure 43. The system essentially consists of two parts, one responding to a situation where the clock is running fast and the other when it is running slow. Gate 1 opens only in the first situation and passes the clock and code second's pulses, each with a frequency of 1 Hz in mode A and 1/60 Hz in mode B. Gate 2, which normally feeds the 1 MHz clock oscillator pulses to the counter, is closed by the clock pulse and reopened by the following code pulse till the two coincide. This effectively stops the oscillator pulses from flowing into the clock counters during the time the clock is running fast and then restarts it in step with the code pulse. Simultaneously, gate 3 opens for the d: . 'on of the error and displays it in a frequency c . ; microseconds.

In a situation where the clock is slow and a given code pulse is ahead of the corresponding clock pulse, the code and the clock pulses pass through gate 4 and not through gate 1. The leading code pulse opens gate 5 and allows additional pulses (the delayed clock oscillator pulses) to flow into the clock counters at the same frequency, till the corresponding clock pulse arives and closes the gate. The additional pulses, fed in for the duration of the

lag, wipe away the error and simultaneously display it in a frequency counter through the logic operation in gate 3.

7.6: Clock Synchronization System Using T.V. Synchronization Pulses.

(C.L.Bhat, I.K.Kaul, R.C.Yadav, M.L.Sapru)

A passive television synchronization system, leading to a relative time accuracy of 1 μs between clocks at Srinagar and Gulmarg, has been developed for the gamma-ray astronomy program at NRL. It utilizes field markers derived from the vertical synchronization pulse train of Srinagar Doordarshan. An absolute time-accuracy of $\leq$ 1ms is simultaneously ensured by the system by allowing independent synchronization of the clocks with the standard high frequency time-code signals from ATA, New Delhi and RWM,Moscow.

A block diagram of the synchronization system is shown in Figure 44 and the detailed circuit diagram in Figure 45. It essentially consists of two input channels, one for absolute time synchronization with radio pulses and the other for relative time synchronization with the T.V. Sync. pulses. The T.V. channel generates 20 ms field markers from the vertical sync. pulses from Srinagar T.V. transmission through the circuit shown in Figure 46. A supplementary detector delivers seconds markers from the 10 MHz time-code signals from ATA, New Delhi or RWM, Moscow (radio markers). The T.V. markers are used by a time synchronizer to monitor and correct the relative time offsets of the two remote clocks, while the ambiguity relative to absolute time is evaluated with the help of radio markers by employing the clock error monitoring

and correction circuit developed for this purpose.

In future, the national T.V. hook-up will enable our synchronization system to be used for achieving an absolute time accuracy of ≤ 10 μs for very long base-line experiments in gamma-ray astronomy.

7.7: Logic System Attached to Low Energy Neutron Pile to Detect Neutrons from Lightning Discharges

(G.N.Shah, H.Razdan, Q.M.Ali, S.R.Kaul, C.L.Bhat)

The Gulmarg neutron monitor (Figure 47) has been modified to record possible neutron bursts from lightning discharges, by removing the lead completely and by incorporating an additional logic system (Figure 26). A dipole antenna in the vicinity of the pile detects the electromagnetic pulse from the lightning discharge, which opens a gate and counts time from a 1 MHz clock till the arrival of the first neutron in the pile. The neutron pulse opens four sequential gates, each of 80 μ s width, during which subsequent neutrons are counted. Any additional neutrons, detected during the four sequential gates of total width 320 μ s, are considered to be a neutron signal from the lightning discharge, as the probability of getting a second cosmic ray produced neutron during this period is negligible. The time delay between the electromagnetic pulse and the first detected neutron is then used to calculate the average distance to the site of neutron generation, after assuming an appropriate energy of the neutron. This mode of recording the neutrons, after the arrival of a precursor electromagnetic pulse from the lightning discharge, helps in achieving a high signal to noise ratio against the cosmic ray background neutrons.

Associated with this system is a logic unit, which counts background electromagnetic pulses produced in the vicinity of the monitor or from lightning discharges between the initial triggering of the system and the completion of neutron counting. This enables us to investigate whether the large time-delay neutron events can be explained on the basis of multi-stroke origin and also helps in eliminating electromagnetic pick up as the origin of lightning generated neutron events. Figure 48 shows the block diagram of the system, which has been designed to record a maximum of four successive electromagnetic pulses and to record their relative time spacings. The circuit essentially consists of three sets of gated decade scalers. The first electrostatic field change due to the lightning discharge triggers the main unit as well as this additional circuit and sets into operation the first set of five gated scalers which count 100 KHz clock pulses. The next pulse closes the first set of scalers and sets into operation the next set of four gated decade scalers and so on. The fourth pulse, or the trailing edge of the last neutron counting gate, whichever is earlier, stops the third set of scalers. From a comparison of this differential time information, with the integral time obtained from the initial triggering of the system and the detection of neutrons, it can be ascertained whether the integral time information really corresponds to the time delay in the arrival of neutrons from the lightning site.

7.8: <u>Development of linear motor systems</u>:
(K.C.Tripathi, P.R.Sarma, M.M.Bemalkhedkar, V.P.Gupta)

Extensive work on the development of unconventional linear and circular motors and motor-

generator systems was initiated in the laboratory in 1974. Initially, a pulsed linear motor with inherent dynamic switching based on entirely new concepts was developed. Figure 49 shows a photograph of the laboratory prototype developed and Figure 50 shows its control circuit. It essentially consists of a track on which are spread ferrite magnets at equal spacing and a carriage which has electromagnets fixed on its underside at the same spacings as the ferrite magnets to ensure proper synchronization. A set of sensor coils are also mounted on the carriage to sense the relative positions of various electromagnets and ferrite magnets and to energise the electromagnets. The electromagnets provide an impulse to the carriage for a duration which varies inherently with its speed and can also be controlled manually to control the speed. This linear motor system is brushless, has high efficiency due to negligible hysterisis loss and pulsed mode of operation and has excellent speed control.

7.9: Development of Circular Motor Systems:
(K.C.Tripathi, P.R.Sarma, V.P.Gupta, A.Karnal)

The linear motor concept has been used to develop a circular motor, in which the ferrite magnets are spread over the periphery of a circular disc, with the electromagnets placed diametrically opposite, as shown in Figure 51 . The torque developed by this motor is proportional to the number of ferrite magnets used. An improved model of this motor has also been developed, in which the ferrite magnets have been replaced by ordinary iron. This system works in the attractional mode, i.e., in each pulse from the sensor coil, the electromagnets attract the iron pieces to produce acceleration. In this system, the

magnetic sensor coils have been replaced by an optical sensor, which has been found to be more exact and efficient. Figure 52 illustrates the characteristics of this motor system.

7.10: On Line Data Processing System for an Energy Dispersive X-ray Fluorescence Spectrometer:

(K.J.S.Sawhney, G.S.Lodha, R.Koul)

An one line data processing system has been designed for an energy dispersive X-ray fluorescence spectrometer using an ECIL make 4K multichannel analyser. The processor analyses the X-ray spectral data and computes the concentration of various trace elements present in the sample. For this purpose, Hindustan Computer Ltd. MICRO 2200 programmable calculator is used. MICRO 2200 basic system has a key board, a display, 18 column printer, 200 data word memory and a programming facility of 2000 program steps. A micro data interface (MDI) of HCL has been attached to MICRO 2200 enabling it to communicate directly with a maximum of four different digital systems and a Floppy diskette of HCL greatly enhances the capability of MICRO 2200 by not only providing mass storage facility but acting also as memory back-up for data and programs. This is possible because the diskette is totally software controlled unlike that of the other conventional systems. The 5" diskette accommodates up to 3000 data words and 30,000 program steps. An interface has been built to couple the MCA and MICRO 2200 which allows the transfer of the four digit address and of the five digit data from MCA to MICRO 2200. For the inverse transfer of data and address from MICRO 2200 to MCA, the inverse data interface has also been built by us.

Software has been developed for data smoothning, background subtraction, peak location, energy calibration, spectrum unfolding and concentration calculations.

7.11: Retriggerable One Shot Protects Three Phase Motors:

(R.Koul, R.C.Yadav)

A simple circuit has been developed which trips a three phase motor in the case of a phase failure and inhibits its reverse rotation in the event of a phase square reversal. The retriggerable one shot, ROS, Figure 53 has a time period of slightly greater than one cycle. The correct phase sequence triggers the ROS after every cycle. However, for any change in phase sequence such triggers are not available and the ROS output gives low, thereby deenergising Relay RL. Failure of V_B switches off RL due to interruption in the low voltage supply. In the event of either or both of the other phases failing the ROS does not get triggered resulting in the tripping of the control relay. The small size of the circuit allows it to be incorporated in the starter of the motor to be protected. The phase sequence part of the circuit can be built into a handy tool for personnel who install three phase distribution systems.

7.12: Thumbwheel Switches Programme Timer:

(R.Koul and G.S.Lodha)

A simple scheme for implementing a programmable timer has been developed for use in an automatic sample changer in the X-ray fluorescence spectrometer set up at NRL. The circuit uses a set of thumbwheel switches and a

multiplexer as its programming elements and allows different samples to be exposed for different preset time intervals. The sample number and the time of its exposure are displayed.

7. Chemistry

7.1: Radiation Chemistry: Wood Plastic Composites

(A.M.Wani, H.M.Gupta, K.N.Rao, Ahinsa Kaul)

A 2300 curie cobalt - 60 gamma radiation source was installed at NRL in 1976, with the specific purpose of investigating and developing wood-plastic composites, the efforts being aimed at developing materials useful for the local industry. Except for Deodar and walnut, all the types of wood found in Jammu and Kashmir are soft and of inferior quality. These woods suffer from such disadvantages like the dimensional instability, hygroscopicity and instability against weather and bacterial attack etc. A program for the study of improvements in the properties of these woods through the production of radiation induced wood-plastic composites was, therefore, started in the laboratory.

The first study on impregnated-irradiated wood was carried out on Poplar (Populus negra) and Wilcow (Salix Fragilis). These woods have a density of 0.35 gm cm^{-3} at a moisture content of 10%. The experiments used methylmethacrylate and vinyl acid as monomer and the dose required for highest polymer conversion (95%) was found to be 3.6 Mrads at 10°C (1.6 Mrads at 25°C). Table 2 lists the important results of this study. It is evident that polymer loading greatly improves the hardness, wear resistance, fire resistance, rate of moisture uptake as well as the aesthetic characteristics of the wood-plastic composite. For example, for 50% polymer loading, hardness increased by a factor of 2.8 for poplar and 3.4 for willow while compression strength increased by a factor of $\sim$ 1.5 for both. The developed wood-plastic composites are found to be better

electric insulators, even at 20% polymer loading. However, the nailability of WPC was found to be poor and samples with $\leq$ 30% polymer loading cracked when a nail of 0.15 cm dia was driven into them.

Further studies have been conducted mainly to produce wood-plastic composites for particular applications like flooring, carving and shingle roofing etc. and to improve the nailability of WPC samples. Samples of wood from fir (Abies pindrow) willow (Salix fragilis), Kail (Betula alnoids) Jangul (Fraxinus) and Deodar and different monomers like styrene, acrylonitrile and methylmethacrylate etc., have been used in these studies. Some of the main results of these studies are:

i) High radiation dose is required for polymerization of styrene due to low radical yield. Dose requirement reduces when styrene is used alongwith carbon tetrachloride or acrylonitrile.

ii) Kail wood requires higher radiation doses compared to other woods, probably because of its higher lignin content.

iii) WPC samples of willow and Jangul, containing 50-60% polymer, are suitable for wood carving as they have good grain structure and aesthetic appearance. A comparison of the properties of various WPC samples and walnut, the wood traditionally used in Kashmir for carving, is shown in Figure 54 . The dotted line represents the properties of walnut wood. It is clear that WPC samples containing 50-60% polymer have the same characteristics as found for walnut wood.

iv) Surface coated wood samples, prepared by applying partially polymerized methylmethacrylate over the wood surface and then fully polymerizing it by thermal

curing, are found most suitable for roofing shingles. The results shown in Table 3 indicate that between surface coated and fully impregnated wood, the former is more suitable for roofing shingles and also requires less quantity of monomer, thus making it cheaper than fully impregnated wood.

v) Deodar PMMA composite, with 50% polymer loading has a high wear index, six times larger than the untreated Deodar, and is found suitable for flooring.

vi) The nailability of WPC samples improves considerably with the addition of 10% ethyl silicate alongwith the monomer. PC samples containing 100% polymer (MMA : ES = 90:10), did not crack when a number of nails of 0.25 cm dia were driven into the samples.

7.2: Panaromic Batch Irradiator Facility

(S.Sabherwal, A.Kaul, A.M.Rani)

Recently, an 80,000 curie cobalt-60 gamma irradiation facility has been installed in the laboratory for conducting radiation processing experiments on a pilot-plant scale. On its shuffle-dwell conveyor system, seven boxes (40x40x40 cm) move around the source array. The irradiation cell is large and gives ample room to accommodate large and heavy objects positioned outside the conveyor system. This pilot plant is expected to serve as a multipurpose facility for wood plastic composite studies, for sterilization of medical products, and for development work on other applications of Co-60 irradiation.

Extensive dosimetry work has been carried out during the commissioning of this facility, the chief objectives being (i) to check that the irradiator is functioning properly and source geometry is correct (ii) to map the pattern of dose distribution within the standard boxes on the conveyor and (iii) to

measure the dwell time required for a minimum dose of 25 K rad (the dose required for sterilization of medical products). Some of the results of this study are shown in Figure 55. A dwell time of 1150 seconds is required to ensure a dose of 2.5 Mrad for a product density of 0.14 grams cm^{-3}, on the conveyor. To ensure that the dosimetric calibration of PANBIT is correct and reliable, intercomparisons using different dosemeters (perspex MX-300, red perspex and cerric-cerrous potentiometric dosemeters) have been carried out. On an experimental basis, the facility has been used for sterilization of a variety of medical products(cotton, guaze, dressings etc.) supplied by local hospitals.

The radiation utulization efficiency of the Panoramic Batch Irradiator is very low (8% at 0.1 gm/cc product density) due to the simple conveyor system used. To study the possibility of increasing the radiation utilization efficiency, dosemetric measurements have been carried out outside the conveyor system. It was found that boxes of the size of 60x60x60 cm could be placed at specific locations outside the conveyor for irradiation. The boxes had to be turned manually on four sides for uniform dose distribution. The overdose ratio was found to be 1.2. The results indicate that the radiation utilization efficiency can be increased to 15% by the optimum use of space available in the radiation cell.

7.3: Atmospheric Chemistry:

(S.Sabherwal, T.N.Das)

An atmospheric chemistry program has been initiated to study the photochemistry of trace species in the atmosphere by monitoring formaldehyde, ozone and oxides of nitrogen. A chemiluminiscent method

for the estimation of low concentration of hydrogen peroxide has been standardised, and Figure 56 shows a schematic view of the system developed for this purpose. The method is based on the chemiluminiscent oxidation of luminol in alkaline medium in the presence of Cu(2) as catalyst. Interference due to dissolved oxygen is eliminated by purging argon through the solution. The lowest detectable concentration of 2×10^{-9} mol cm^{-3} was found to be limited by the background concentration of hydrogen peroxide present in triple distilled water, used for making the solutions. Preliminary observations taken at Gulmarg agree with our earlier conclusion that cloud cover decreases the formation of formaldehyde and hydrogen peroxide, while at the same time increasing the life-time of these species in the atmosphere due to their slower photodecomposition.

Table 1

Number of neutrons per event	Number of Events			
	MT	%	LT	%
1	8,299	98.84	10,818	96.65
2	97	1.11	250	2.23
3	4	0.05	40	0.35
> 3	0	0.00	84	0.76

TABLE 2

RELATIVE MERITS OF DIFFERENT POLYMERS IN IMPROVING THE PROPERTIES OF POPLAR AND WILLOW WOOD

S.No.	Sample	Impregnant	% polymer loading	Wear improvement factor	Impact strength J	Hardness	% water absorption 12 dayss	Compression strength in 10 Pa
1.	Poplar	Nil	0	1	1.67	8	42	220
2.	Poplar	MMA	100	3.5	1.87	39	22	380
3.	Poplar	15% VA + 85% MMA	100	3.4	1.97	37	40	379
4.	Poplar	30% VA + 70% MMA	100	3.2	1.97	35	35	372
5.	Poplar	VA	100	2.9	1.95	28	45	344
6.	Willow	Nil	0	1.0	1.83	8	133	220
7.	Willow	MMA	90	4.4	1.90	43	33	421
8.	Willow	15% VA + 85% MMA	90	4.2	1.93	40	39	407
9.	Willow	30% VA +	90	4.11	1.91	38	47	392
10.	Willow	VA	90	3.9	1.90	35	52	365

TABLE 3

COMPARISON OF PROPERTIES OF SURFACE COATED WOOD AND WPC

Monomer = MMA

Wood = Willow

S.No.	Wood Sample	% volume swollen in 20 days	% water observed in 20 days	Temperature difference at 2cm (thermal insulation test)	% change in hardness (severe climatic condition test	%weight loss after treatment with	
						3.6 N H_2SO_4	2.5 N NaOH
1.	WPC with 100% polymer	3.81	40.0	6.2	4.4	17.8	20.8
2.	Surface coated wood	0.25	15.2	7.2	0.5	8.8	9.1

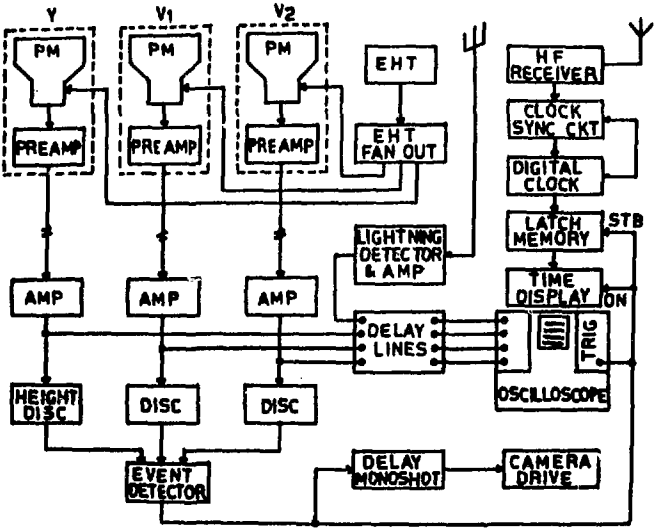
V
V1
V2
PM
PM
PM
EHT
HF RECEIVER
PREAMP
PREAMP
PREAMP
EHT FAN OUT
CLOCK SYNC CKT
DIGITAL CLOCK
LATCH MEMORY
STB
LIGHTNING DETECTOR & AMP
TIME DISPLAY
ON
AMP
AMP
AMP
DELAY LINES
TRIG
OSCILLOSCOPE
HEIGHT DISC
DISC
DISC
EVENT DETECTOR
DELAY MONOSHOT
CAMERA DRIVE

Fig. 1

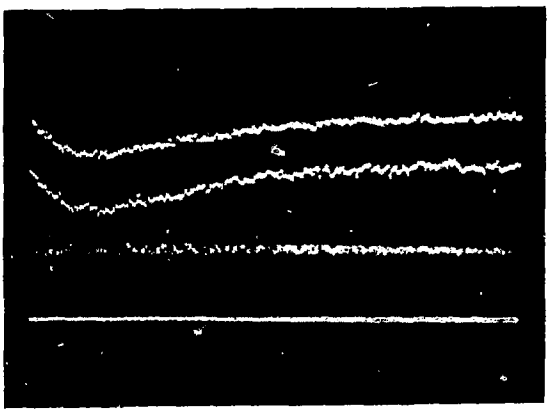

Fig. 2

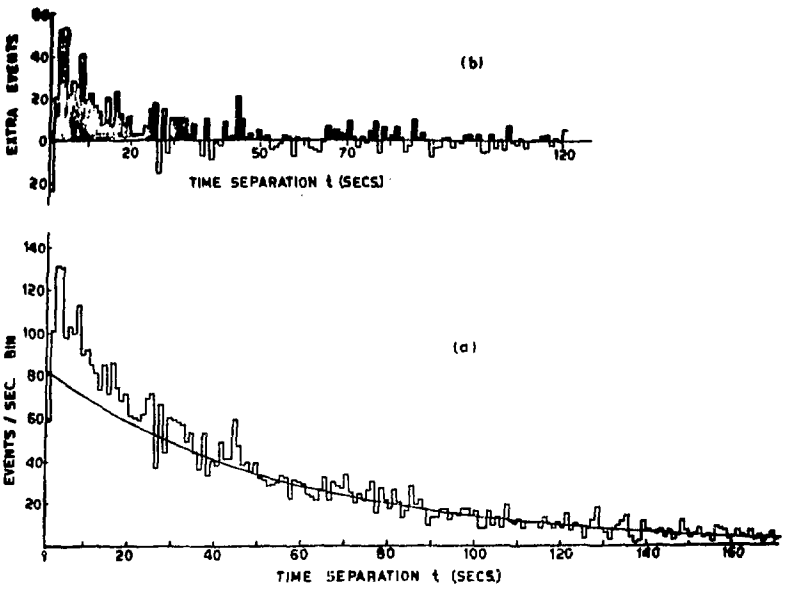
EXTRA EVENTS
(b)
TIME SEPARATION t (SECS)
EVENTS / SEC. BIN
(a)
TIME SEPARATION t (SECS)

Fig. 3

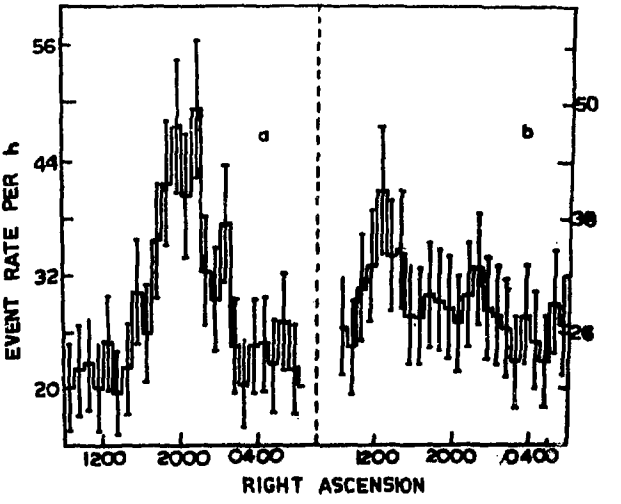
EVENT RATE PER h
a
b
RIGHT ASCENSION

Fig. 4

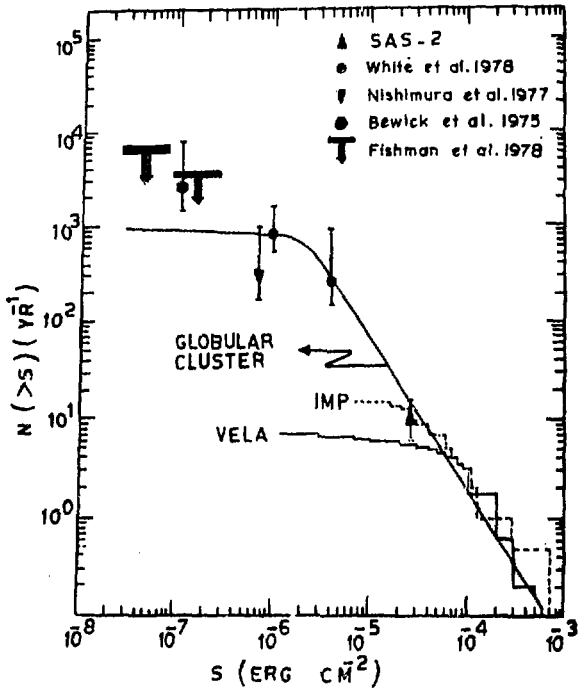
SAS-2
White et al. 1978
Nishimura et al. 1977
Bewick et al. 1975
Fishman et al. 1978
GLOBULAR CLUSTER
IMP
VELA
N (>S) (YR⁻¹)
S (ERG CM⁻²)

Fig. 5

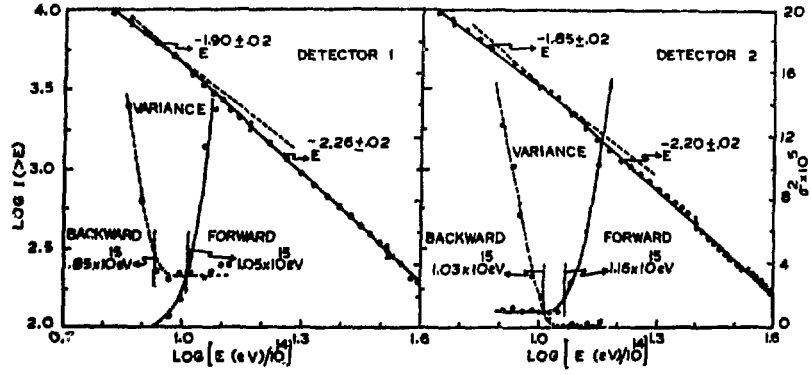
DETECTOR 1
DETECTOR 2
VARIANCE
BACKWARD
FORWARD
LOG I (>E)
LOG [E (eV)/10]

Fig. 6

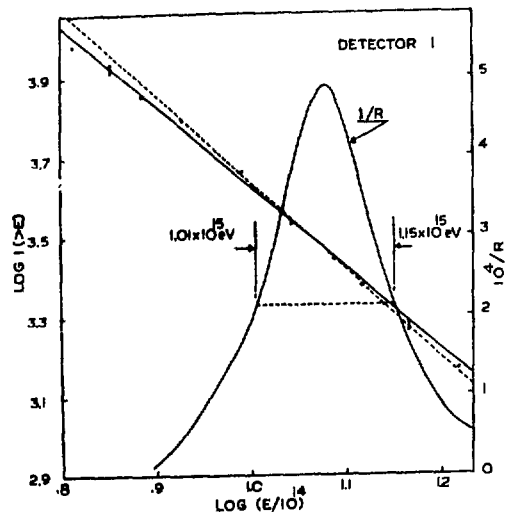

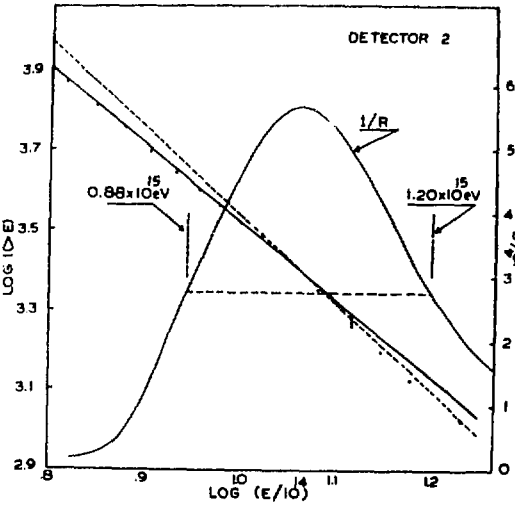

Fig. 7

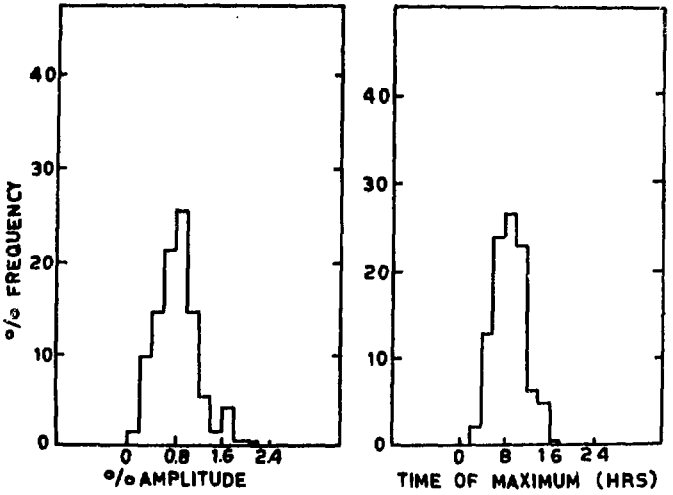

Fig. 8

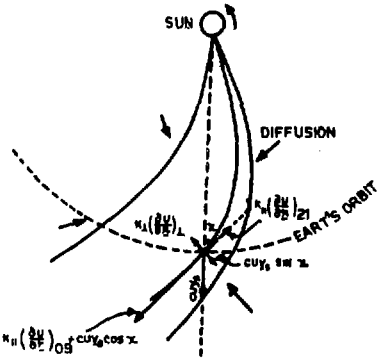

Fig. 9

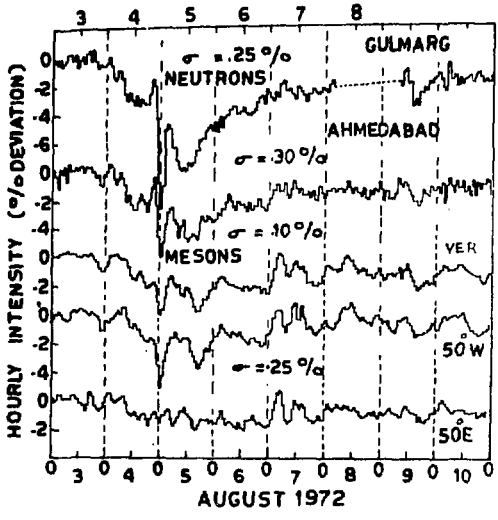

Fig. 10

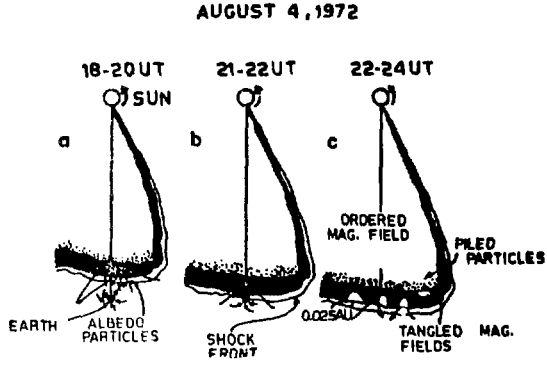

Fig. 11

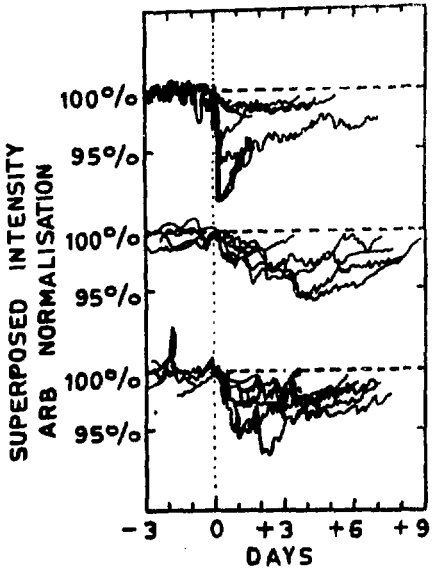

Fig. 12

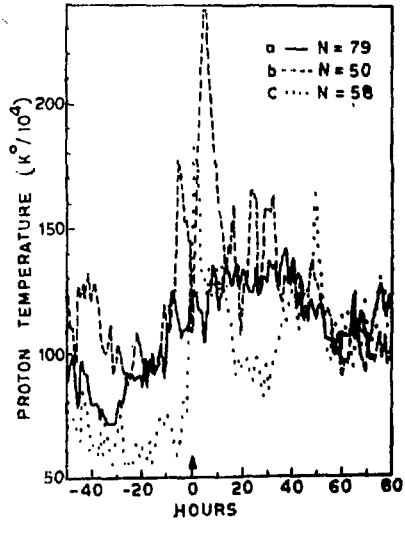

Fig. 13

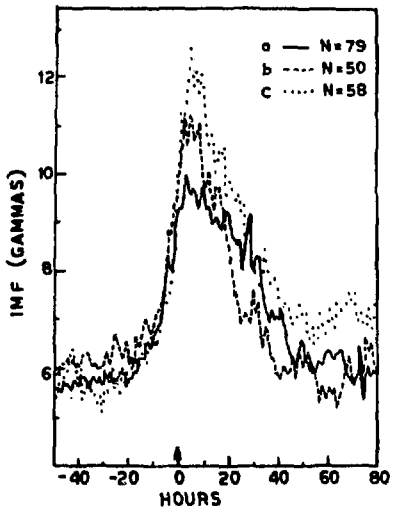

Fig. 13

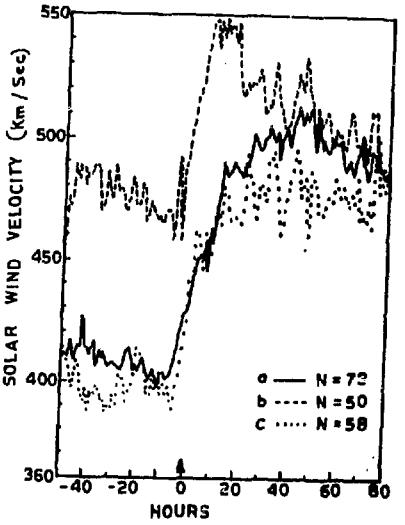

Fig. 13

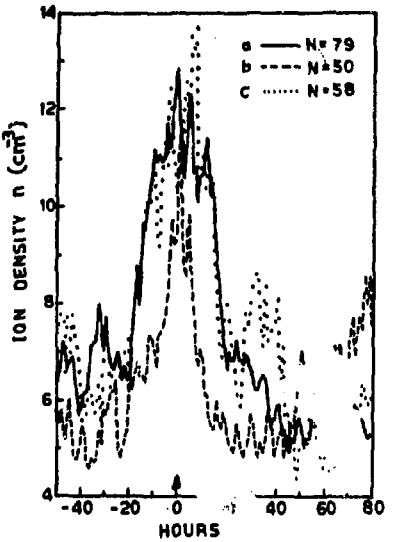

Fig. 13

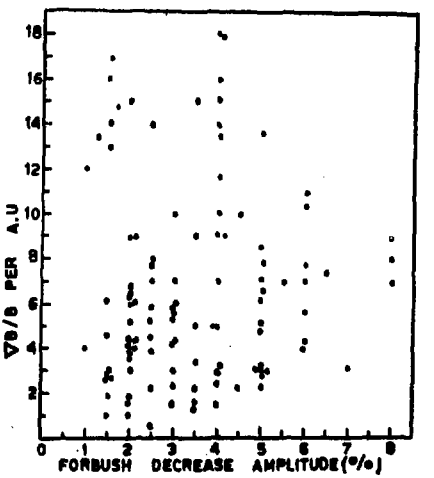

Fig. 14

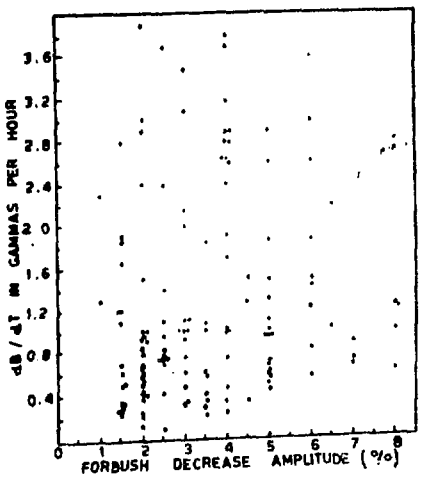

Fig. 15

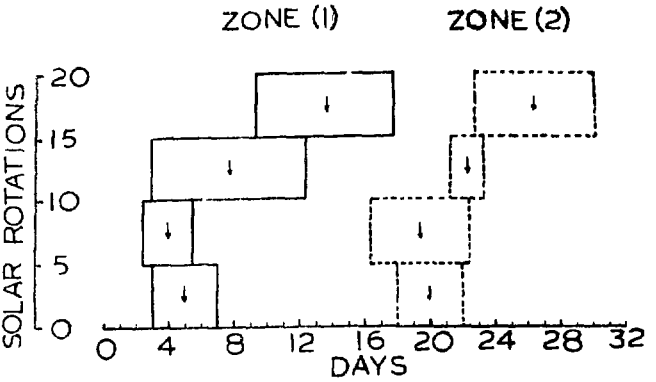

Fig. 16

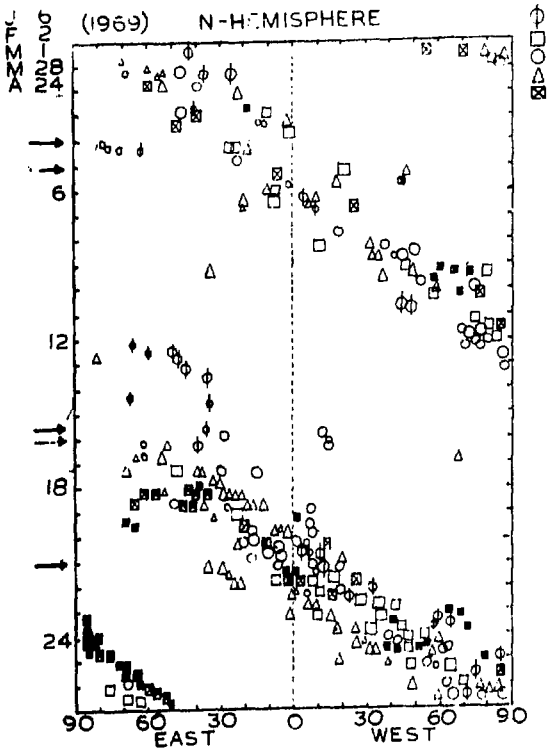

Fig. 17

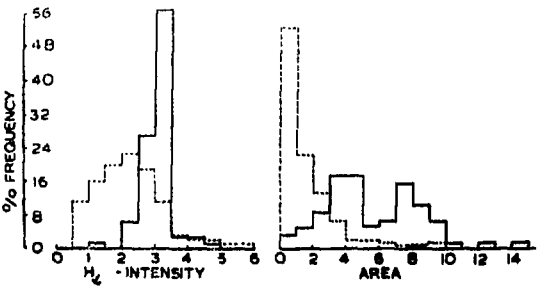

Fig. 18

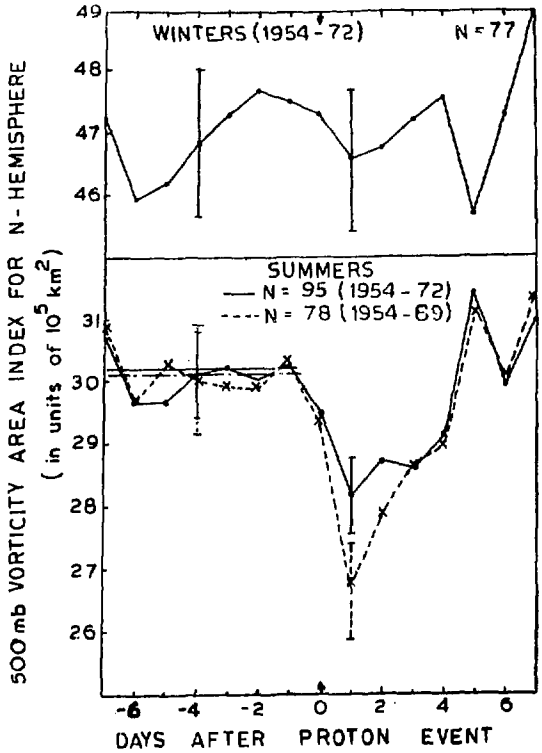
WINTERS (1954-72)
N = 77
SUMMERS
N = 95 (1954-72)
N = 78 (1954-69)
500 mb VORTICITY AREA INDEX FOR N-HEMISPHERE
(in units of 10^5 km^2)
DAYS AFTER PROTON EVENT

Fig. 19

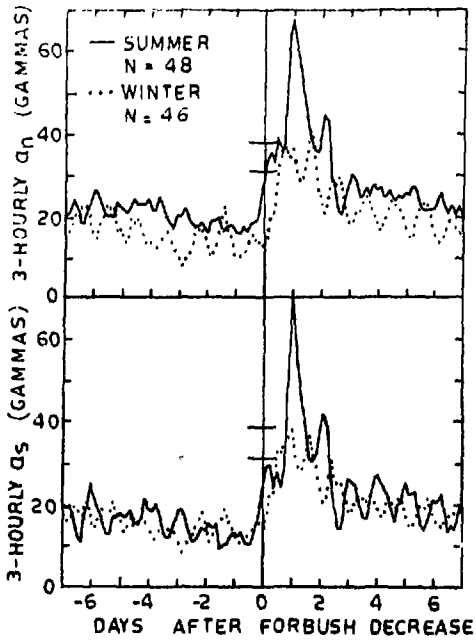
SUMMER
N = 48
WINTER
N = 46
3-HOURLY a_n (GAMMAS)
3-HOURLY a_s (GAMMAS)
DAYS AFTER FORBUSH DECREASE

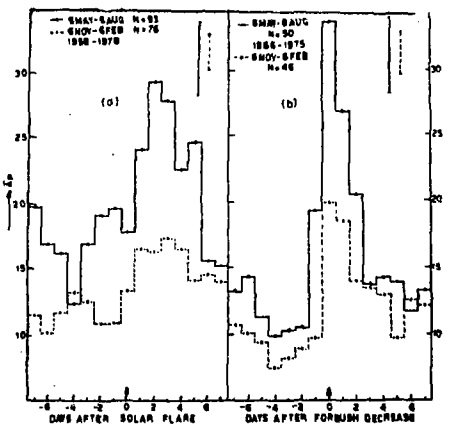
DAYS AFTER SOLAR FLARE
DAYS AFTER FORBUSH DECREASE

Fig. 20

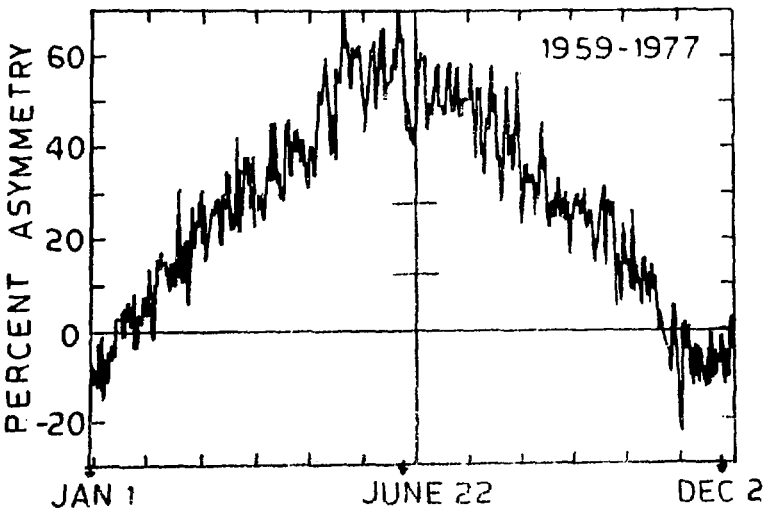

Fig. 21

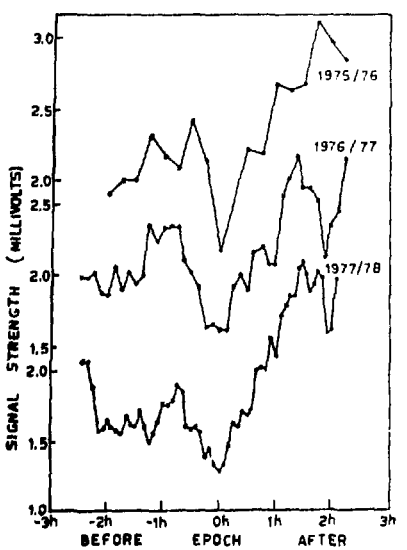

Fig. 22

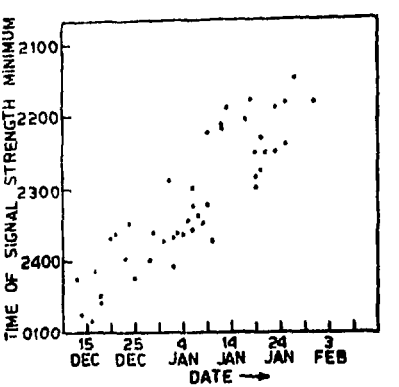

Fig. 23

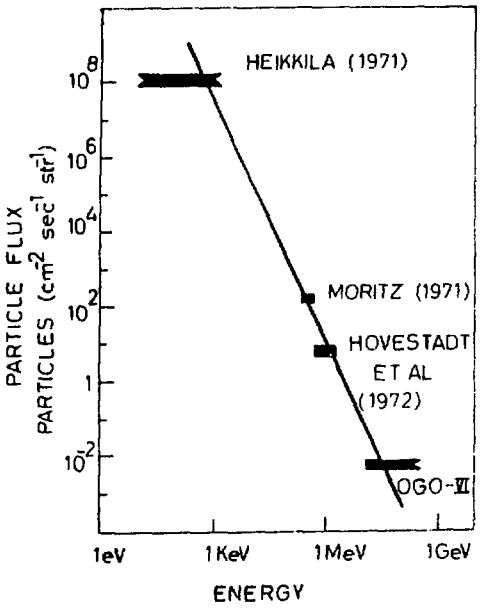

Fig. 24

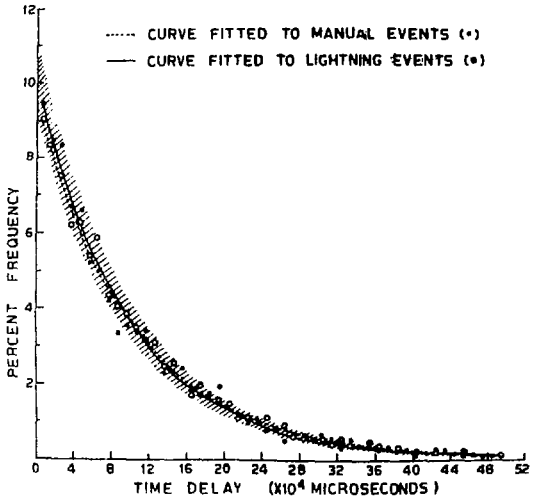

Fig. 27

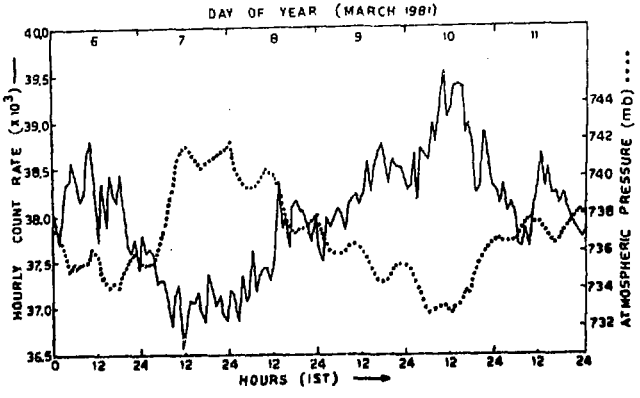

Fig. 25

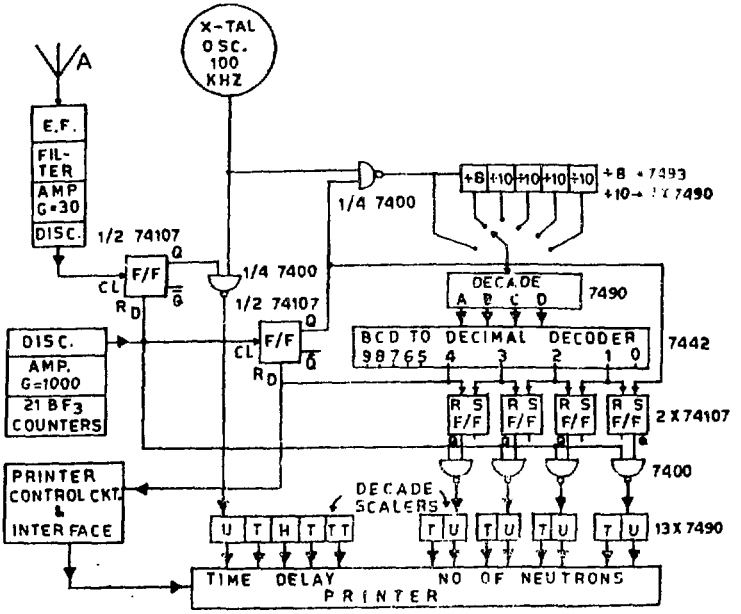

Fig. 26

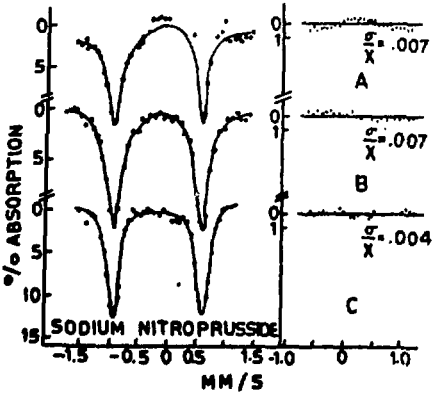

Fig. 28

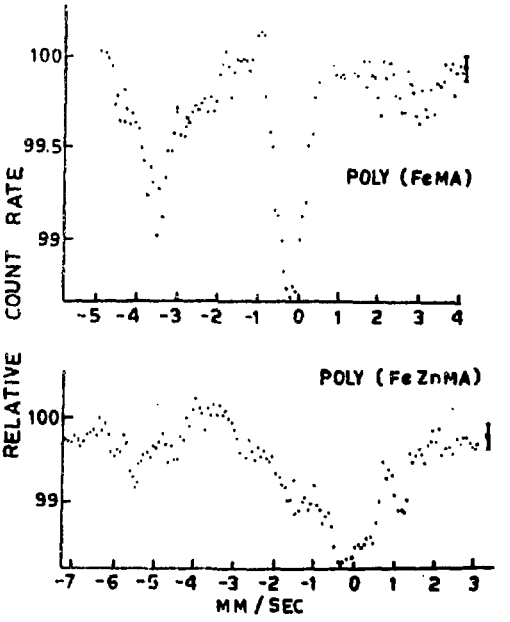

Fig. 29

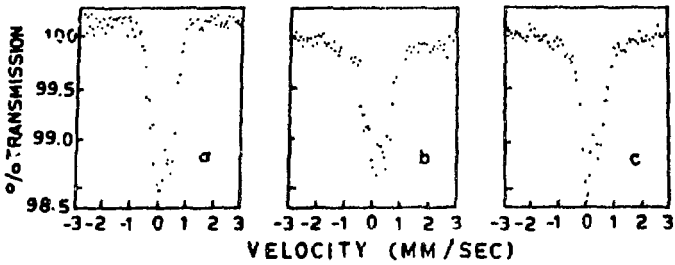

Fig. 30

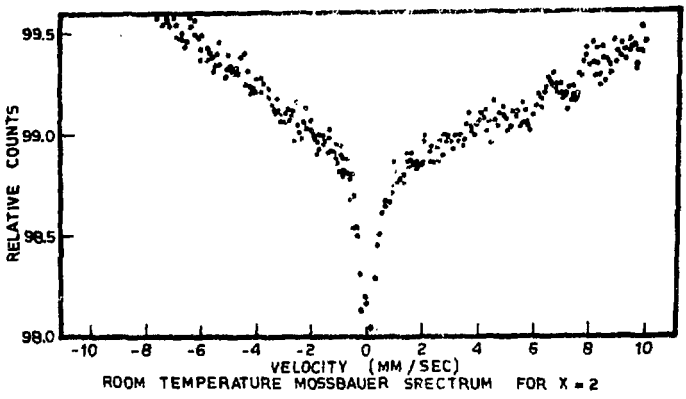

Fig. 31

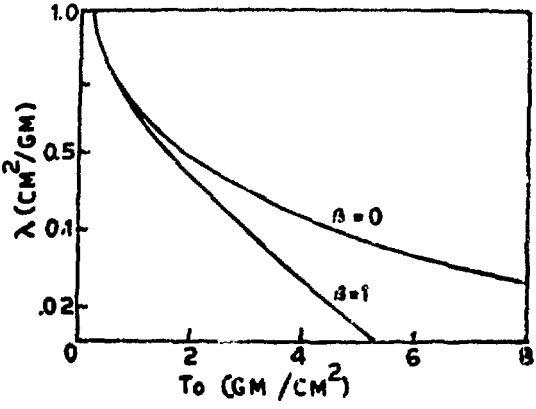

Fig. 32

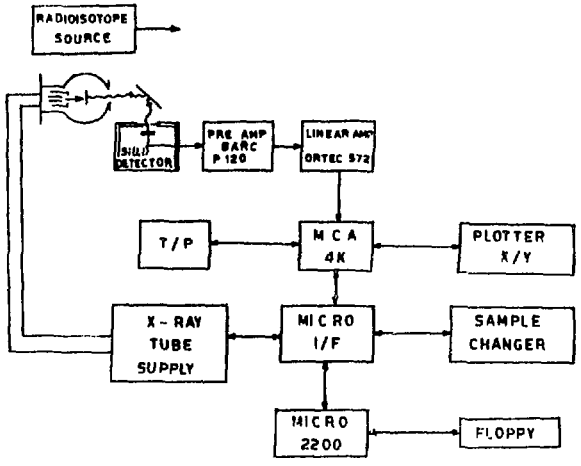

Fig. 33

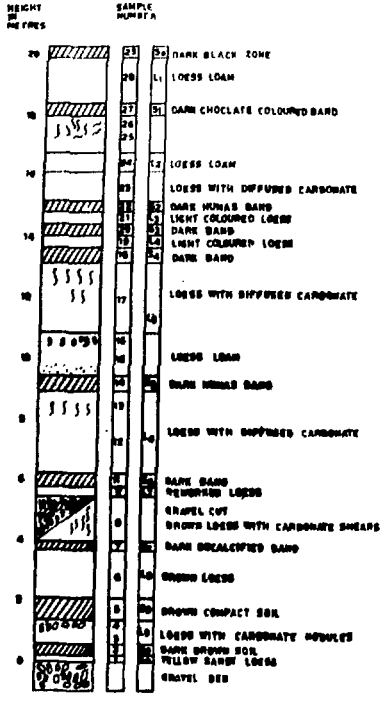

Fig. 34

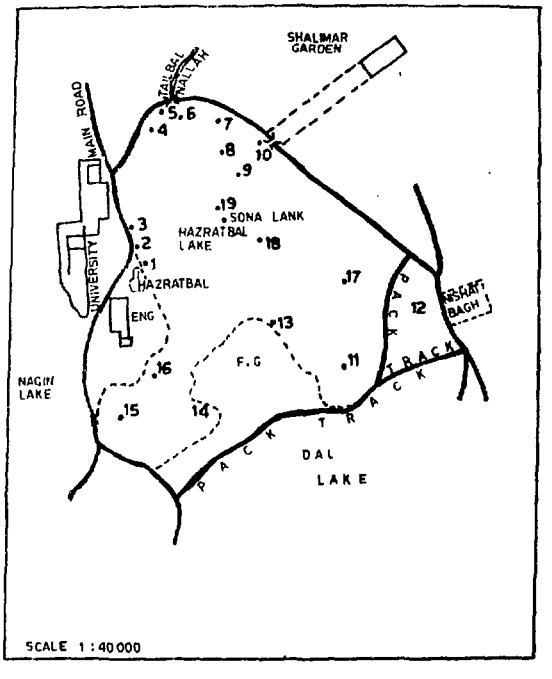

Fig. 35

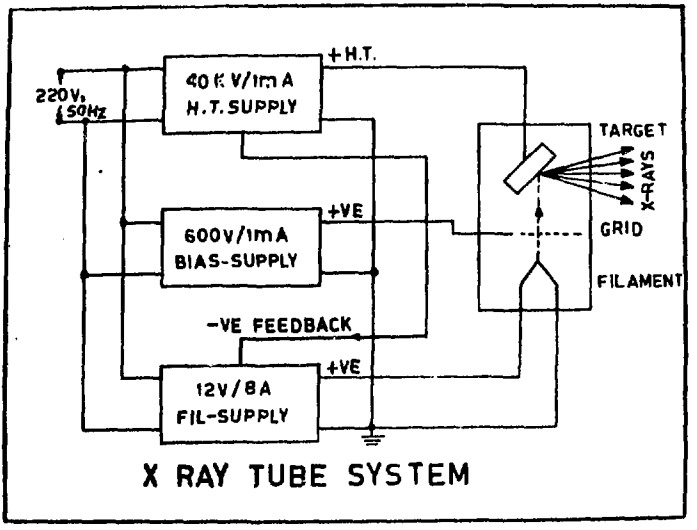
220V, 50Hz
40 K V/1m A
H.T. SUPPLY
+H.T.
600V/1mA
BIAS-SUPPLY
+VE
-VE FEEDBACK
12V/8A
FIL-SUPPLY
+VE
TARGET
X-RAYS
GRID
FILAMENT
X RAY TUBE SYSTEM

Fig. 36

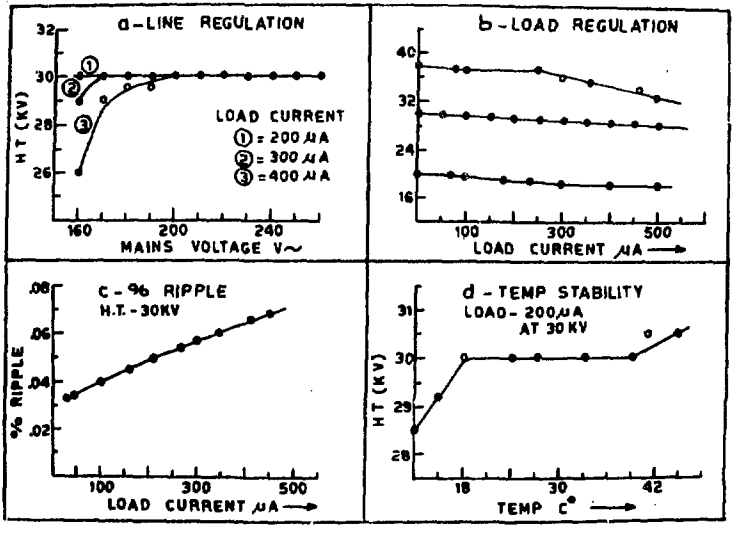
a - LINE REGULATION
H T (KV)
LOAD CURRENT
① = 200 μA
② = 300 μA
③ = 400 μA
MAINS VOLTAGE V~
b - LOAD REGULATION
LOAD CURRENT μA
c - % RIPPLE
H.T. - 30KV
% RIPPLE
LOAD CURRENT μA
d - TEMP STABILITY
LOAD - 200 μA
AT 30 KV
H T (KV)
TEMP C°

Fig. 37

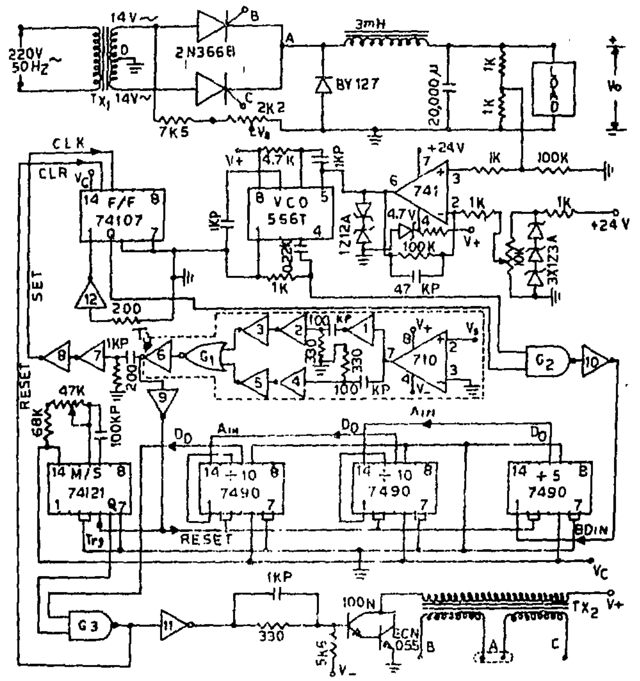
220V 50Hz~
14V~
2N3668
BY127
3mH
20,000μ
1K
LOAD
V_o
7K5
2K2
CLK
CLR
SET
RESET
F/F 74107
VCO 566T
741
710
+24V
100K
1Z12A
3X1Z3A
M/S 74121
÷10 7490
÷5 7490
G1
G2
G3
BCN 055
TX2
ALL INV 7404
NAND 7400
NOR 7402
V+ = +12V
V– = –12V
V_C = +5V

Fig. 38

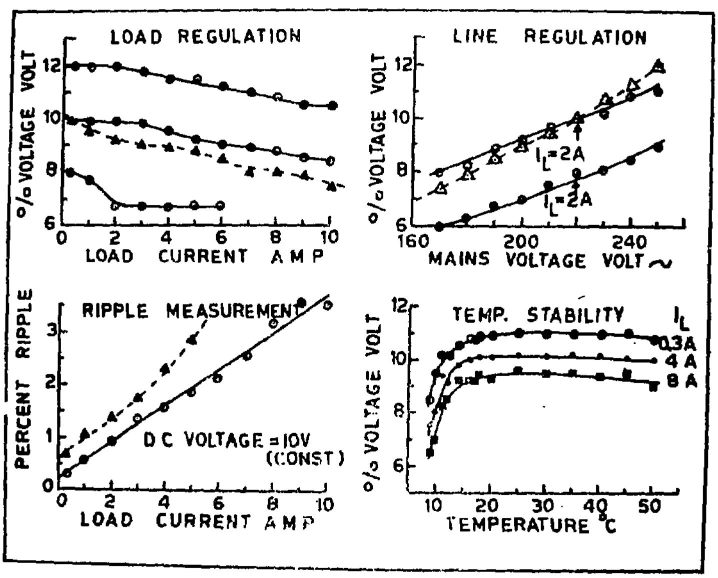
LOAD REGULATION
% VOLTAGE VOLT
LOAD CURRENT AMP
LINE REGULATION
I_L=2A
MAINS VOLTAGE VOLT~
RIPPLE MEASUREMENT
PERCENT RIPPLE
DC VOLTAGE =10V (CONST)
TEMP. STABILITY
I_L
0.3A
4A
8A
TEMPERATURE °C

Fig. 39

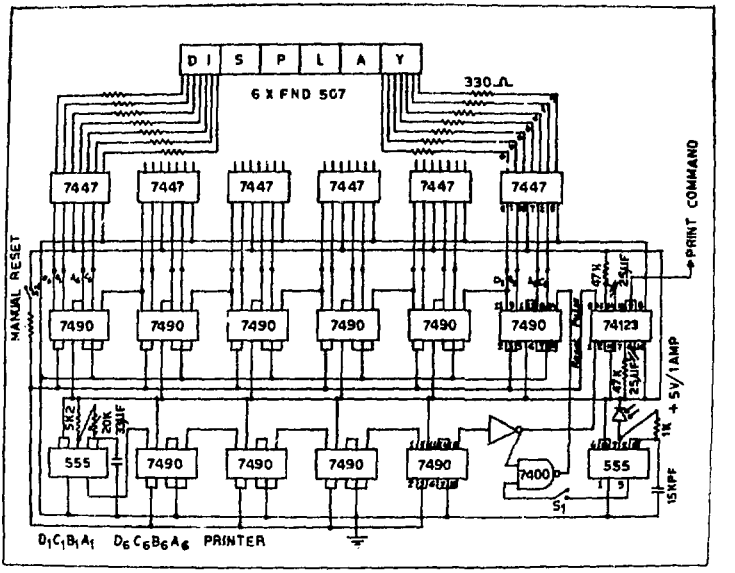
DISPLAY
6 X FND 507
330Ω
7447
7490
74123
555
7400
MANUAL RESET
PRINT COMMAND
+5V/1AMP
PRINTER

Fig. 40

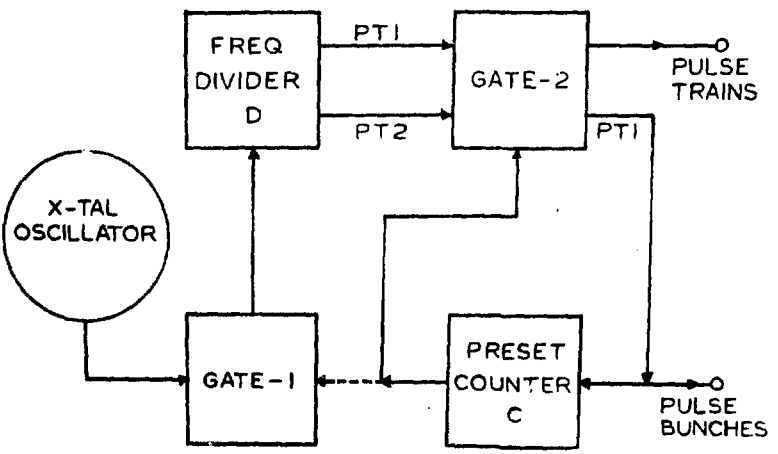
FREQ DIVIDER D
PT1
PT2
GATE-2
PULSE TRAINS
PT1
X-TAL OSCILLATOR
GATE-1
PRESET COUNTER C
PULSE BUNCHES

Fig. 41

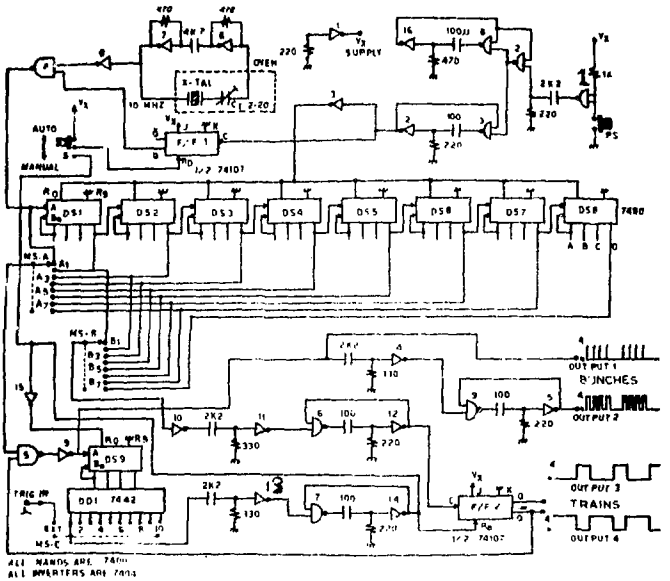
AUTO
MANUAL
OUTPUT 1
BUNCHES
OUTPUT 2
OUTPUT 3
TRAINS
OUTPUT 4

Fig. 42

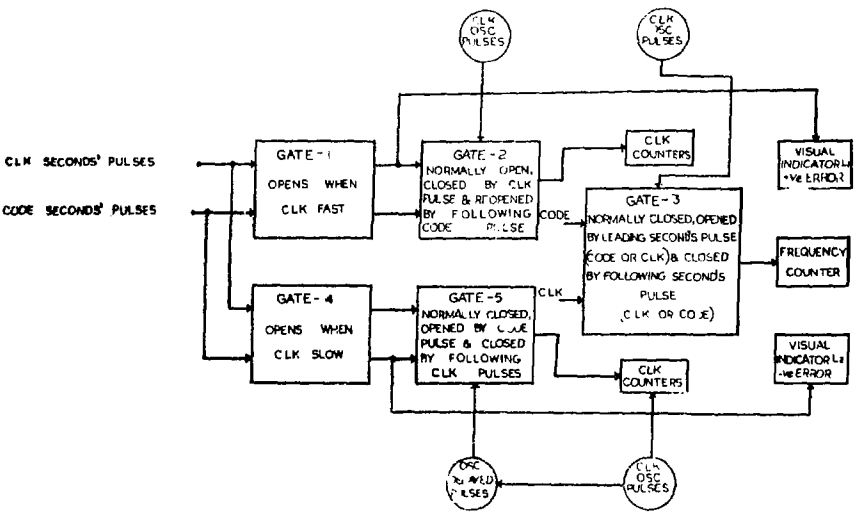
CLK SECONDS' PULSES
CODE SECONDS' PULSES
GATE - 1
OPENS WHEN
CLK FAST
GATE - 2
NORMALLY OPEN,
CLOSED BY CLK
PULSE & REOPENED
BY FOLLOWING
CODE PULSE
CLK
OSC
PULSES
CLK
OSC
PULSES
CLK
COUNTERS
VISUAL
INDICATOR
+Ve ERROR
GATE - 3
NORMALLY CLOSED, OPENED
BY LEADING SECONDS PULSE
(CODE OR CLK) & CLOSED
BY FOLLOWING SECONDS
PULSE
(CLK OR CODE)
CODE
FREQUENCY
COUNTER
GATE - 4
OPENS WHEN
CLK SLOW
GATE - 5
NORMALLY CLOSED,
OPENED BY CODE
PULSE & CLOSED
BY FOLLOWING
CLK PULSES
CLK
CLK
COUNTERS
VISUAL
INDICATOR
-Ve ERROR
OSC
PULSES
CLK
OSC
PULSES

Fig. 43

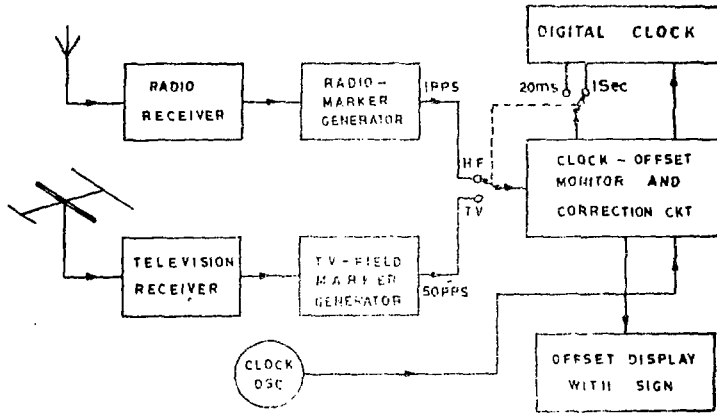

Fig. 44

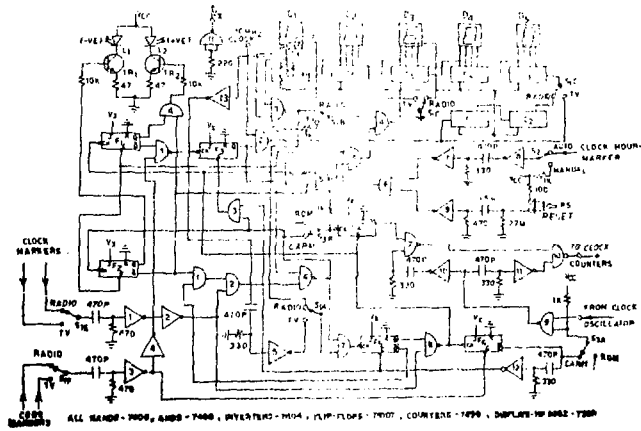

Fig. 45

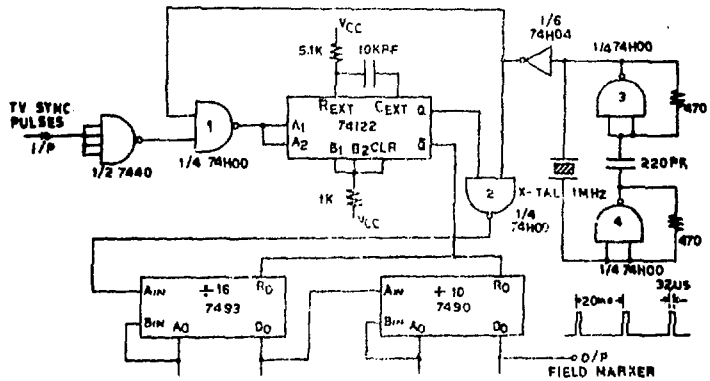

Fig. 46

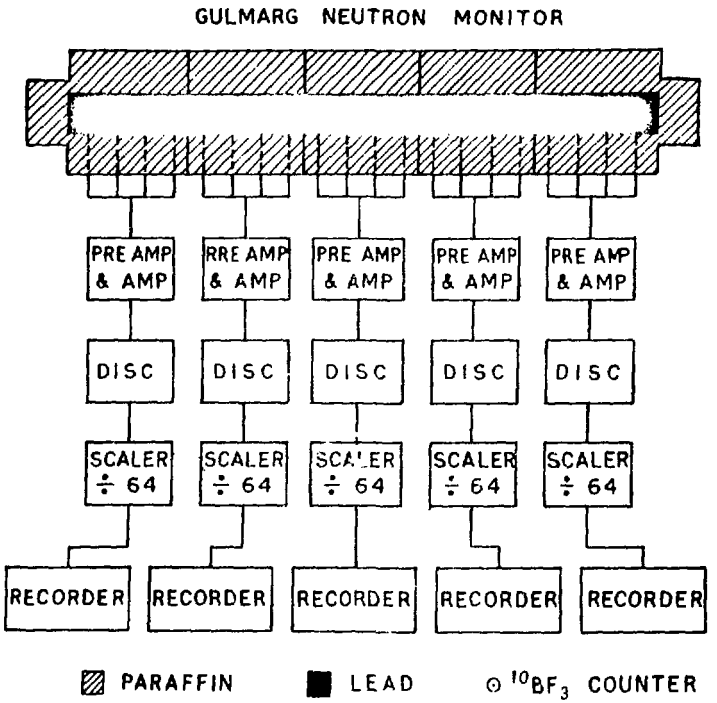
GULMARG NEUTRON MONITOR
PRE AMP & AMP
RRE AMP & AMP
PRE AMP & AMP
PRE AMP & AMP
PRE AMP & AMP
DISC
DISC
DISC
DISC
DISC
SCALER ÷ 64
SCALER ÷ 64
SCALER ÷ 64
SCALER ÷ 64
SCALER ÷ 64
RECORDER
RECORDER
RECORDER
RECORDER
RECORDER
PARAFFIN
LEAD
$^{10}BF_3$ COUNTER

Fig. 47

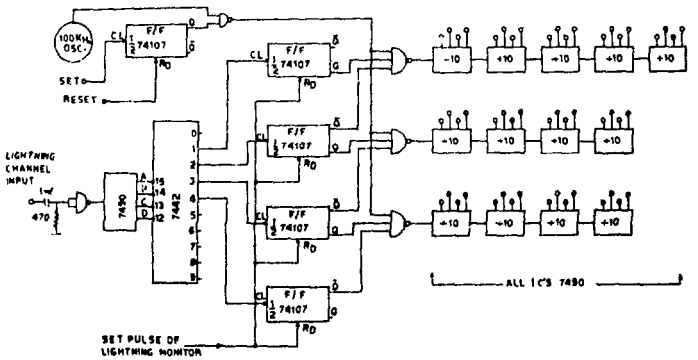
100KHz OSC.
F/F 74107
SET
RESET
LIGHTNING CHANNEL INPUT
7490
7442
÷10
ALL IC'S 7490
SET PULSE OF LIGHTNING MONITOR

Fig. 48

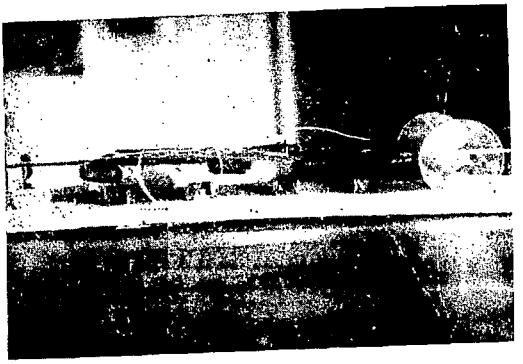

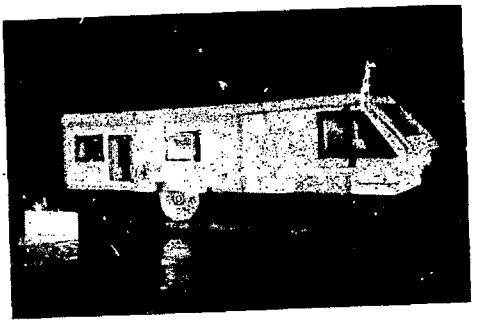

Fig. 49

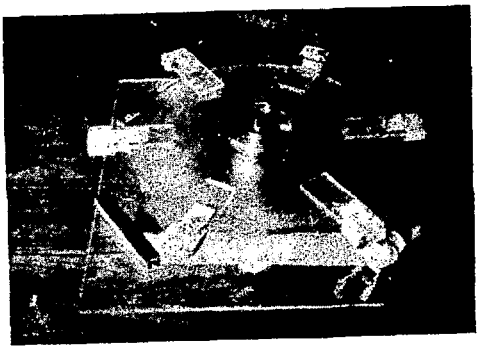

Fig. 51

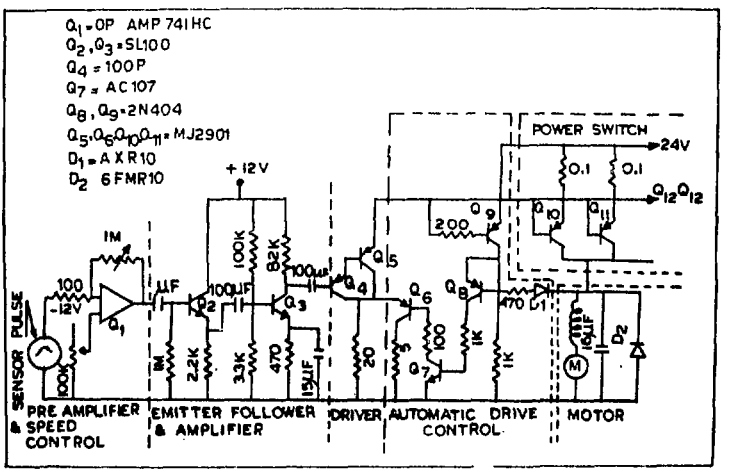

Fig. 50

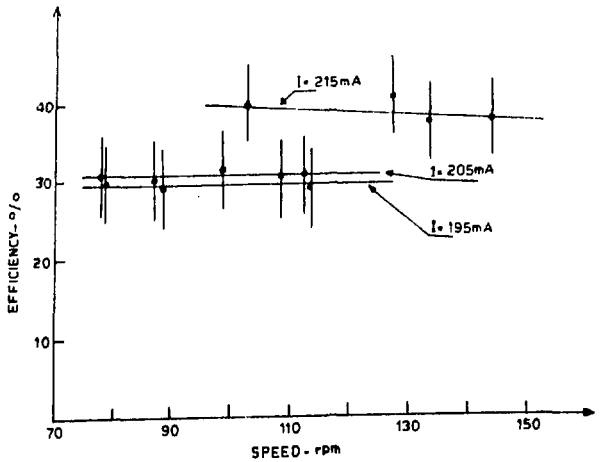

Fig. 52

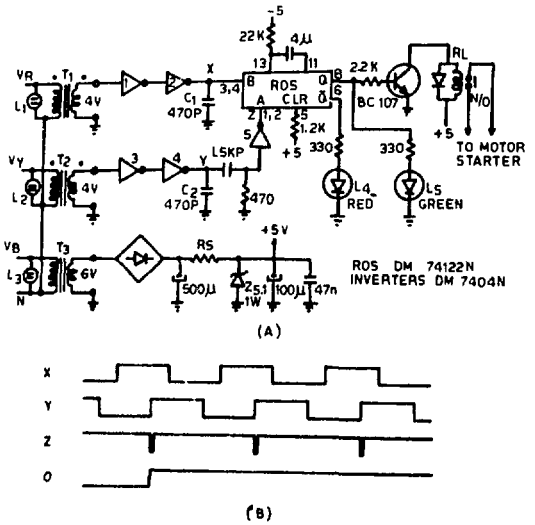

Fig. 53

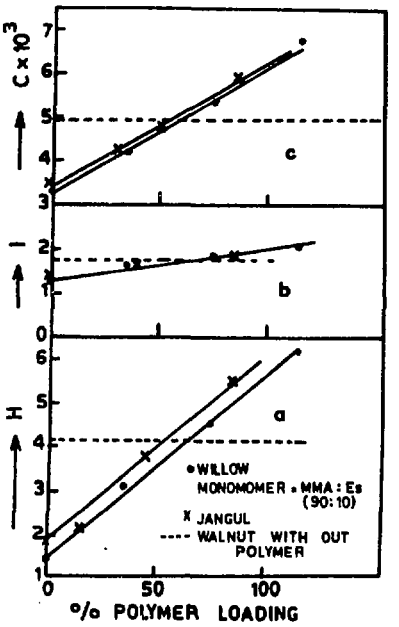

Fig. 54

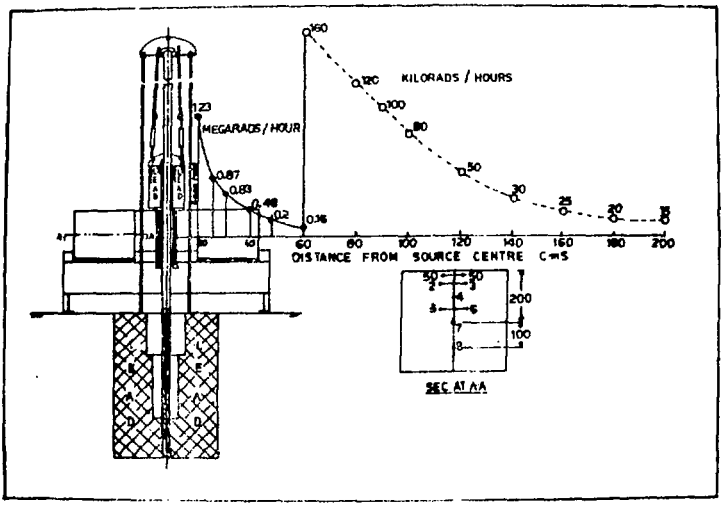
KILORADS / HOURS
MEGARADS / HOUR
DISTANCE FROM SOURCE CENTRE Cms
SEC AT AA

Fig. 55

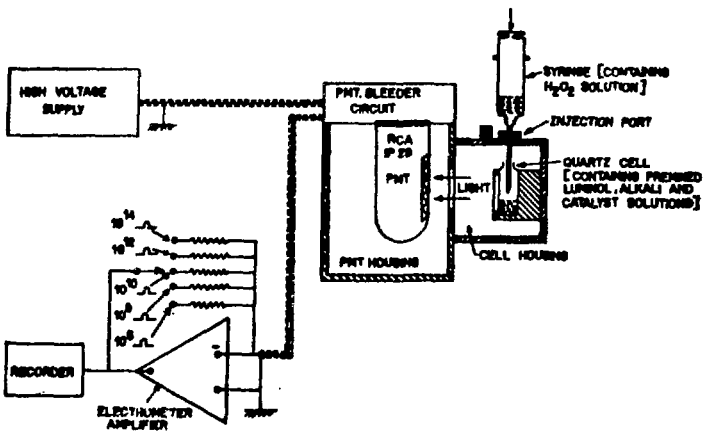
HIGH VOLTAGE SUPPLY
PMT. BLEEDER CIRCUIT
RCA IP 29
PMT
LIGHT
PMT HOUSING
SYRINGE [CONTAINING H_2O_2 SOLUTION]
INJECTION PORT
QUARTZ CELL [CONTAINING PREMIXED LUMINOL, ALKALI AND CATALYST SOLUTIONS]
CELL HOUSING
RECORDER
ELECTROMETER AMPLIFIER

Fig. 56

List of Published Papers from NRL (1974-1985)

A. Space Physics

1. High Energy Cosmic Ray Intensity Increases of Non-Solar Origin and the Unusual Forbush Decrease of August 1972, S.P.Agrawal, A.G.Ananth, M.M.Bemalkhedkar, L.V.Kargathra, U.R.Rao and H.Razdan, Journal of Geophysical Research, 79, 2269, 1974

2. Low Energy Charged Particle Ring Around Equator in the Altitude Range 400-1100 Km., R.K.Kaul, H.Razdan and J.A.Lockwood, Astrophysics and Space Sciences, 46, 215, 1977.

3. Distribution of Active Regions on the Sun, G.N.Shah, H.Razdan and C.L.Kaul, Indian Journal of Radio and Space Physics, 6,307, 1977

4. Recurrent Forbush Decreases and the Relationship Between Active Regions and M-Regions, G.N.Shah, C.L.Kaul, H.Razdan & M.M.Bemalkhedkar, Journal of Geophysical Research, 83,3740,1978.

5. Cosmic Ray Measurements on a Polar Orbiting Satellite, R.K.Kaul, Indian Journal of Physics, 52B,344, 1978

6. Geomagnetic Activity and the Effect of Tau X-1 on Lower Ionosphere, R.K.Kaul and H.Razdan, Indian Journal of Radio and Space Physics, 8,414,1979.

7. A Non-Random Component in Cosmic Rays of Energy $\geq 10^{14}$ eV, C.L.Bhat, M.L.Sapru and C.L.Kaul, Nature, 288,146, 1980.

8. A New Upper Limit on Optical Bursts from Primordial Black Hole Explosions, C.L.Bhat, H.Razdan and M.L.Sapru, Astrophysics and Space Science, 73,513, 1980

9. The Type Dependence of SFA at Low Frequencies, R.K.Kaul, Indian Journal of Radio and Space Physics, 55B,435, 1981

10. Short-Term Stability of ATA Time-Signals, C.L.Bhat, R.C.Yadav, S.K.Kaul, M.M.Bemalkhedkar and R.K.Kaul, Journal of the Institution of Electronics and Telecommunication Engineers, 27, 553, 1981.

11. Solar Proton Events and Terrestrial Weather, G.N.Shah,Journal of Atmospheric and Terrestrial Physics, 43, 147, 1981.

12. Cosmic Gamma-rays - Present Status and Future Prospects, H.Razdan, Proc. Indian National Science Academy, 47A, 99, 1981

13. Cosmic Ray Diurnal Anisotropy During Feb.- March, 1977 R.K.Kaul,Indian Journal of Radio and Space Physics,11,88, 1982.

14. Solstitial and Hemispherical Asymmetry in the Response of Geomagnetic Field, G.N.Shah,, R.K.Kaul, H.Razdan, C.L. Kaul, W.M.Wilcox, W.J.Merryfield, Journal of Geophysical Research, 89,295, 1984

15. A Very Long Base-Line Search for Correlated Air Showers From Relativistic Dust Grains, C.L.Bhat, H.S.Rawat, H.Razdan, M.L.Sapru and S.C.Tonwar, Journal of Physics G:Nucl. Phys., 10, 1771, 1984.

16. Neutron Generation in Lightning Bolts, G.N.Shah, H.Razdan, C.L.Bhat and Q.M.Ali, Nature,313,773, 1985.

17. Evidence for a Non-Magnetospheric Origin of Fast Atmospheric Pulsations (FAP), C.L.Bhat, M.L.Sapru and R.K.Kaul, To appear in Journal of Geophysical Research, 1985.

18. Response of Atmospheric Lightnings to Systematic Changes in the Global Electric Field, C.L.Bhat, M.L.Sapru, R.K.Kaul, and H.Razdan, Communicated to Journal of Geophysical Research, 1985.

19. Pulsed Flux of $\geq 10^{14}$ eV Gamma-Rays from Cygnus X-3,C.L.Bhat M.L.Sapru and H.Razdan, Communicated to Astrophysical Journal, 1985.

Nuclear and Solid State Physics

1. Mossbauer Studies on Polymetallomethacrylates, K.C.Tripathi, P.R.Sarma and H.M.Gupta, Journal of Polym. Sci.,Polym.Lett. Ed., 16, 629, 1978.

2. A Constant Velocity Mossbauer Spectrometer Free of Long-Term Instrumental and Radioactive Decay Drifts, P.R.Sarma, A.K.Sharma and K.C.Tripathi, Nuclear Instruments and Methods, 164, 591, 1979.

3. Mossbauer Study of the Gamma-Induced Polymerization of Iron Methacrylate, P.R.Sarma, K.C.Tripathi and H.M.Gupta, Journal of Polymer Sciences, Polymer Chemistry Ed.,18, 2609, 1980.

4. Optimization of Absorber Thickness for Improving the Quality of a Mossbauer Spectrum, P.R.Sarma, Ved Prakash and K.C.Tripathi, Nuclear Instruments and Methods, 178, 167, 1980.

5. Modification of the Parameters of a Mossbauer Source due to Self Absorption Effects, P.R.Sarma and K.C.Tripathi, Nuclear Instruments and Methods, 226, 463, 1984.

C. Electronics and Technical Physics

1. An error monitoring and correction circuit for clocks, C.L.Bhat, H.Razdan, M.L.Sapru and I.K.Kaul, Journal Inst. of Electronics and Telecom. Engs., 24, 9, 1978.

2. A clock synchronization circuit using transmitted time-codes, C.L.Bhat and H.Razdan, Defence Science Journal, 28, 153, 1978.

3. A battery run pulsed linear motor and its electronic control system, K.C.Tripathi, P.Lal, M.M.Bemalkhedkar, P.R.Sarma and N.Tyle, IEEE Trans. on IECI, 25, 293, 1978

4. A digital electronic timer, C.L.Bhat and R.Koul, Journal Inst. of Engs., 59, 57, 1979.

5. Wide range pulse generator displays timing parameters, C.L.Bhat and R.C.Yadav, Electronics, 52, 128, 1979.

6. An error - monitoring and correction circuit (a modification), C.L.Bhat, I.K.Kaul and M.L.Sapru, Journal Inst. of Electronics and Telecom. Engs., 25, 167, 1979.

7. Novel motor systems with inherent dynamic switch control for transport and other purposes, K.C.Tripathi, V.P.Gupta, P.R.Sarma and A.K.Sharma, BARC Tech. Rept, No.1027, 1979

8. An inexpensive digital pulse generator, C.L.Bhat and R.C.Yadav, Journal Inst. of Engrs., 60, 93, 1980

9. A battery run pulsed motor with inherent dynamic electronic switch control, K.C.Tripathi, P.Lal, P.R.Sarma, A.K.Sharma and V.P.Gupta, IEEE Trans. on IECI, 27, 29, 1980.

10. Time synchronization system in a two-station search for primordial black holes, C.L.Bhat, I.K.Kaul and R.C.Yadav, Journal Inst. of Electronics and Telecom. Engs., 27, 1981. 556

11. Thumbwheel switches programme timer, R.Koul and G.S.Lodha, Journal Inst. of Electronics and Telecom. Engs., 27, 1981.

12. Regulated DC power supply employs digital control for firing its SCR's, M.M.Bemalkhedkar, R.Koul, C.M.Tripathi and M.S.Qureshi, Journal Inst. of Electronics and Telecom. Engs. 27, 220, 1981.

13. Circuit identifies radio-time minute to correct clock time offset, C.L.Bhat and R.C.Yadav, Journal Inst. of Engrs. 62,61, 1982.

14. An integrated, stabilized power supply for x-ray tubes, M.M.Bemalkhedkar, C.M.Tripathi, M.N.Kumbhare and H.S.Vora, Journal Inst. of Electronics and Telecom. Engs., Tech Rev., 1, 133, 1984.

15. Photo on/off with SCR as GTO, H.S.Vora, M.N.Kumbhare and M.M.Bemalkhedkar, To appear in Electronic Engineering.

16. SCR-regulated, variable DC power supply with fixed sampling ratio, M.M.Bemalkhedkar, C.M.Tripathi and M.N.Kumbhare, To appear in EDN.

List of Papers Presented at Conferences, Symposia, Workshops etc.

A. Space Physics

1. Preliminary Results from the Atmospheric Fluorescence Detector at Gulmarg , C.L.Bhat, R.K.Kaul and H.Razdan, National Symp. on High Energy Physics, Calcutta, 1974.

2. On Detection of Cosmic Gamma-Ray Bursts through Atmospheric Fluorescence, C.L.Bhat, M.L.Sapru and H.Razdan, Bulletin Astronomical Society of India. 4,87, 1976,

3. On the Location of M-regions on the Sun, G.N.Shah, C.L.Kaul, M.M.Bemalkhedkar and H.Razdan, Proc. Solar Planetary Physics Symp., Ahmedabad, 2, 27, 1976.

4. Charged Particle Ring Around Equator in the Altitude Range 400-1100 Km., R.K.Kaul, H.Razdan, J.A.Lockwood, Solar and Planetary Physics Symposium Ahmedabad, 2, 187 ,1976.

5. Cosmic Ray Diurnal Vector During the 1976 Solar Activity Minimum, R.K.Kaul, H.Razdan, M.M.Bemalkhedkar and C.L.Bhat, 15th Int. Cosmic Ray Conf., Sofia, 4 ,23, 1977.

6. Evidence for Steepening of Primary Cosmic Ray Energy Spectrum Near 10^{15} eV from a Cerenkov Detection System at Gulmarg,, C.L.Bhat, H.Razdan, P.R.Sarma and M.L.Sapru, 15th Int. Cosmic Ray Conf., Sofia, 8,508, 1977.

7. Possible Gamma-Burst Events with an Associated High Energy Component, C.L.Bhat, H.Razdan, M.L.Sapru and Ved Prakash, Bull. Astronomical Society of India, 6, 47, 1978.

8. Origin of Millisecond Atmospheric Fluorescence Events Recorded at Gulmarg, C.L.Bhat, H.Razdan and M.L.Sapru, Bull. Astronical Society of India, 6, 48, 1978.

9. Pulsed Emission from Atmospheric Nitrogen at Low Latitudes, C.L.Bhat, H.Razdan and M.L.Sapru, Radio and Space Sciences Symp., New Delhi, ,1979.

10. Forbush Decreases and Interplanetary Magnetic Blobs, G.N.Shah, C.L.Kaul and H.Razdan, Radio and Space Sciences Symp., New Delhi, 1979.

11. Forbush Decreases, Coronal Holes and Solar Wind Streams, G.N.Shah, C.L.Kaul and H.Razdan, Radio and Space Sciences Symp.,New Delhi, 1979.

12. Geomagnetic Activity and the Effect of Tau X-1 on the D-Region, R.K.Kaul and H.Razdan, Radio and Space Sciences Symp.,New Delhi, 1979.

13. Forbush Decreases, Flares and Recurrent Streams, G.N.Shah, C.L.Kaul and H.Razdan, 16th Int. Cosmic Ray Conf., Kyoto, 3,423, 1979.

14. Possible Origin of Cosmic Gamma-ray Bursts in Globular Clusters, H.Razdan and C.L.Bhat, 16th Int. Cosmic Ray Conf., Kyoto, ,1, 236,, 1979.

15. A Non-Random Contribution to $\geq 10^{14}$ eV Energy Cosmic Rays on the Time Scale of a fraction of a Minute, C.L.Bhat, P.R.Sarma, M.L.Sapru and C.L.Kaul,, 16th Int. Cosmic Ray Conf., 857, 1979.

16. Cosmic Optical Bursts and a New Upper Limit for Primordial Black Hole Explosions, C.L.Bhat, H.Razdan and M.L.Sapru 16th Int. Cosmic Ray Conf., Kyoto,2, 17, 1979.

17 A Search for Cosmic Optical Bursts of Nanosecond Duration, C.L.Bhat, H.Razdan and M.L.Sapru, National Space Sci., Symp., Varanasi, 1980.

18. A Search for Time Correlated Ultra High Energy ($\geq 10^{14}$ eV) Gamma-Rays, C.L.Bhat, M.M.Bemalkhedkar, H.Razdan and M.L.Sapru, National Space Sci. Symp., Varanasi, 1980.

19. A Proposed Balloon Search for Cosmic Optical Pulses of Nanosecond Time Scale, C.L.Bhat, M.M.Bemalkhedkar, C.L.Kaul and H.Razdan, Workshop on Opportunities for High Altitude Balloon Experiments in India,,Hyderabad, 1980.

20. On Cosmic Origin of Atmospheric Fluorescence Pulses Recorded at Gulmarg, C.L.Bhat, H.Razdan and M.L.Sapru, 17th Int. Cosmic Ray Conf., Paris, 1, 73, 1981.

21. Atmospheric Fluorescence Pulse Profiles for Impulsive X-and Gamma-ray Bursts, C.L.Bhat, S.K.Kaul, C.L.Kaul and M.L.Sapru, ,17th Int. Cosmic Ray Conf., Paris, 1,73, 1981.

22. Microsecond Time Scale Optical Pulses Detected at Gulmarg and Srinagar, C.L.Bhat, M.L.Sapru, H.Razdan and C.L.Kaul, 17th Int. Cosmic Ray Conf., Paris, 1, 77, 1981.

23. Causes of Forbush Decreases, G.N.Shah, C.L.Kaul, H.Razdan and S.R.Kaul, 17th Int. Cosmic Ray Conf., Paris, 7, 21, 1981.

24. Asymmetry in Geomagnetic Field Response to Solar Disturbances, G.N,.Shah, C.L.Kaul and H.Razdan, Proc. Symp. on Interdisciplinary Approaches to Geomagnetism, Bombay, 1,259, 1981.

25. Evidence of Thermonuclear Neutrons in the Atmospheric Lightning, G.N.,Shah, H.Razdan, C.L.Bhat,, Q.M.Ali and S.R.Kaul, Proc. National Space Sciences Symp., Bangalore, 3, 414, ,1982.

26. Optical Lightnings as a Background in Searches for Cosmic X-and Gamma-ray Bursts through Atmospheric Fluorescence, C.L.Bhat, R.K.Kaul and M.L.Sapru, 18th Int. Cosmic Ray Conf., Bangalore, 8 ,32, 1983.

27. Lead-Free Neutron Monitor Detects Neutrons from Lightning Bolts, G.N.Shah, H.Razdan, C.L.Bhat, Q.M.Ali and S.R.Kaul, Proc. 18th ICRC, Bangalore, 3,555,1983.

28. Fluorescent Light from Cosmic Air Showers, C.L.Bhat, V.K.Sanecha, A.K.Mitra, M.L.Sapru and H.Razdan, Proc. 18th ICRC, Bangalore,11 ,416,1983.

Nuclear and Solid State Physics

1. Mossbauer Study of Copolymers of Iron and Nickel Methacrylates in Methacrylic Acid, P.R.Sarma, K.C.Tripathi and H.M.Gupta, Proc. Nucl. Phys. and Solid State Phys. Symposium, India, 22C,600,1979.
2. Electrical Conduction in the Copolymers of Iron and Nickel Methacrylates in Methacrylic Acid, P.R.Sarma, K.C.Tripathi, H.M.Gupta, Ved Prakash and A.K.Sharma, Proc. Nucl. Phys. and Solid State Phys. Symposium, India, 22c, 256, 1979.
3. Mossbauer Study of Radiation Initiated Polymerization of Iron Acrylate, P.R.Sarma, H.M.Gupta, and K.C.Tripathi, Proc. Int. Conf. on Applications of Mossbauer Effect, Jaipur, India, 1981.
4. Thickness Dependence of the Line Width of a Scattering Mossbauer Spectrum, P.R.Sarma and M.R.Singh, Proc. Nucl. Phys. and Solid State Phys. Symp. India, 25C,248, 1982.
5. A Semi-Automatic Energy Dispersive X-ray Fluorescence Spectrometer; It's Development and Applications to Elemental Analysis in Various Fields, G.S.Lodha and R.Koul, Int. Symp. on Trace Analysis and Technological Development, India, 1981.
6. Trace Elements in the Kanchinala (Kashmir) Loess Deposits, G.S.Lodha, K.J.S.Sawhney, H.Razdan and M.Lal, in "Climate and Ecology of Kashmir: Last 4 Million Years", Ed. by D.P.Agrawal, Today and Tomorrow's Printers and Publishers, 1983.
7. Concentration Profile of Elements in Dal Lake Sediments, G.S.Lodha, K.J.S.Sawhney, H.Razdan, National Workshop on Conservation of Dal Lake, Srinagar, 1983.
8. On-Line Data Processing System for an Energy Dispersive X-ray Fluorescence Spectrometer, K.J.S.Sawhney, G.S.Lodha, and R.Koul, National Sym. on Instrumentation, Srinagar, 1984.

9. Energy Dispersive X-ray Fluorescence and its Application in Geosciences, G.S.Lodha, Workshop on Activation Analysis, Calcutta, 1984.

10. Paleoclimatic Studies on Kashmir Loess, D.P.Agrawal, N.Juyal, Sheela Kusumgar, G.S.Lodha and H.Razdan, Int. Conf. on Paleoclimatic Studies , Poland, 1985.

C. Electronics and Technical Physics

1. Some unconventional linear and rotary motor systems with electronic control for transport purposes, K.C. Tripathi and V.P.Gupta, Symp. on Optimum/alternate utilization of energy in automobiles, Ahmednagar, 1981.
2. Inherent dynamically switched pulsed dc motors and possible simultaneous motor-generator systems, K. C. Tripathi and V.P.Gupta, Seminar on proof and evaluation of vehicles and subsystems, Ahmednagar, 1984.
3. Development of a digital photometer system for ambient visible photon flux measurements, H.S.Vora, T.N.Das and M.N,Kumbhare,,National Symp. on Instrumentation, 1984.